IEEE Access
Multidisciplinary ⋮ Rapid Review ⋮ Open Access Journal

Received 31 August 2023, accepted 13 September 2023, date of publication 22 September 2023,
date of current version 27 September 2023.

Digital Object Identifier 10.1109/ACCESS.2023.3318112

RESEARCH ARTICLE

High-Accuracy, High-Gain Phased Array Utilizing Matrix-Sum and Tunable Amplifier Techniques

YI-TING LIN[1], (Graduate Student Member, IEEE), ZUO-MIN TSAI[1], (Senior Member, IEEE), AND JEN-MING WU[2], (Senior Member, IEEE)

[1]Institute of Communications Engineering, College of Electrical and Computer Engineering, National Yang Ming Chiao Tung University, Hsinchu 30010, Taiwan
[2]Institute of Communications Engineering, Department of Electrical Engineering, National Tsing Hua University, Hsinchu 30013, Taiwan

Corresponding author: Zuo-Min Tsai (zuomintsai@gmail.com)

This work was supported in part by the Co-Creation Platform of the Industry-Academia Innovation School, National Yang Ming Chiao Tung University (NYCU), under the framework of the National Key Fields Industry-University Cooperation and Skilled Personnel Training Act, from the Ministry of Education (MOE) and industry partners in Taiwan, Ministry of Science and Technology, under Grant 111-2223-E-A49-003-MY3, Grant 109-2221-E-009-124-MY3, Grant 112-2218-E-110-002, Grant 112-2218-E-002-031, and Grant 111-2623-E-A49-008; and in part by the Taiwan Semiconductor Research Institute (TSRI).

ABSTRACT This paper presents an 8-element phased array system and proposes a novel beam control method—namely, matrix-sum method—that can achieve beam steering and beam-width control. The system architecture comprises an 8×8 phase matrix network and a 1-to-8 real number weighting network. The 1-to-8 real number weighting network simultaneously supplies the required weighting value to all input ports of the phase matrix network, enabling the adjustment of the phase difference and power ratio between adjacent output signals and thereby generating the desired beam. According to the equations used to calculate the weighting values, the matrix-sum method requires only real number weighting to achieve beam synthesis with steering and tapering functions if used with a suitable phase matrix. Comparison results revealed that for the same number of control bits, the proposed method system exhibited higher beam-steering accuracy and system gain in different beam pattern cases than phased array systems that use conventional and vector-sum phase shifters. The proposed phased array system was fabricated and experimentally investigated at 3.5 GHz. The results indicated that it achieved fully controllable beam steering with a fine beam resolution of 1° steps. Additionally, the system's sum, difference, and tapering beam patterns were accurate compared with ideal beam patterns.

INDEX TERMS Beamforming system, beam steering, beam tapering, phased array, sum and difference beam patterns.

I. INTRODUCTION

Phased array system has become critical in various applications, including fifth-generation (5G), beyond 5G communication, and radar. Its beamforming function improves communication quality, spectral efficiency, and tracking accuracy [1], [2], [3], [4], [5], [6], [7], [8], [9]. Additionally, the electronic beam steering capability provides greater advantages to current satellite communication (SATCOM) systems (low earth orbit (LEO) and medium-earth orbit (MEO)) compared to previous mechanical solutions like dishes mounted on motorized pedestals [10], [11], [12].

In a phased array system, precisely controlling the amplitude and phase of the RF signal fed to each antenna is essential for achieving the desired beam pattern; this is because the accuracy of the phase and amplitude adjustments governs the deviation and resolution of the beam angle [13], [14], [15]. The flexibility of phase shifting and amplitude weighting in an array determines the properties of the beam patterns produced by the array, such as the beam angle range, beam width, and beam type (e.g., sum or difference beam pattern). Thus, a phased array system must be able to

The associate editor coordinating the review of this manuscript and approving it for publication was Giorgio Montisci.

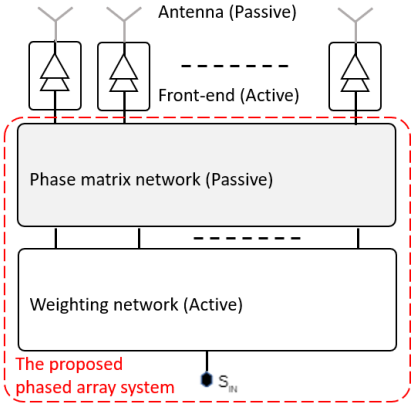

FIGURE 1. Concept of implementing the proposed phased array system on a narrow beam transmitter.

accurately and effectively adjust the phase shift and amplitude weighting.

In the architecture of phased array systems, conventional phase shifters, including switched filter type [16], [17], [18], [19], [20] and reflective type [21], [22], [23], [24], [25], are typically used for phase control, while the amplitude controllers, such as variable gain amplifiers and attenuators, are used for amplitude control. Although this architecture enables separate controlling of the phase and amplitude, the resolution of conventional phase shifters considerably affects the beam resolution [26]. For example, phased array systems using conventional 6-bit controlled phase shifters can achieve 1.8° beam angle resolution when the beam angle is near 0°. However, this resolution deteriorates to over 3° as the beam angle deviates to 90°. This separate control necessitates more calibration. In addition, magnitude control introduces phase errors, and phase control results in magnitude errors, further complicating the calibration procedure.

Vector-sum phase shifters [27], [28], [29], [30], [31] are an alternative to conventional phase shifters and can simultaneously control phases and amplitudes by weighting the in-phase and quadrature-phase (IQ) signals, respectively. Vector-sum phase shifters have a high resolution, high accuracy, and wide bandwidth. Moreover, vector-sum phase shifters require only a 4-bit amplitude controller to achieve nearly the same beam resolution (1.8°) as conventional phase shifters with 6-bit controlled. However, a vector-sum phase shifter includes at least one quadrature phase generator, one power combiner, and one phase inverter, resulting in an unavoidable 6 dB distribution loss. This unavoidable loss leads to at least a 6 dB decrease in the overall system power budget in a phased array system.

This paper proposes a novel phased array system that uses the matrix-sum method to control the final relative phase and amplitude of each array element. The matrix-sum method enables the phased array system to achieve a higher accurate beam steering within 1° beam angle resolution when compared to systems using conventional or vector-sum phase shifters with the same number of control bits. The weighting network in the proposed architecture is realized using 1-to-2 tunable amplifiers, which avoid the distribution losses for different beam cases. Fig. 1 illustrates the implemented concept in a large-scale array transmitter utilizing the proposed phased array system. The system comprises four main parts (weighting network, phase matrix network, front-end, and antenna); these parts can be fabricated using specific processes to enhance performance and cost-effectiveness. For example, the weighting network can be implemented using the CMOS process, optimizing both area requirements and power consumption. The phase matrix network and antenna can be fabricated using the low-temperature co-fired ceramic (LTCC) process, ensuring efficient heat dissipation. Additionally, the front-end part can be realized using the GaAs process to achieve higher output power. Because most of the large-area passive parts in the proposed system can be implemented using low-cost passive processes such as LTCC process, the area of integrated circuits can be minimized. References [32], [33], [34], and [35] depict that the realization of high-frequency passive components and amplifiers are commonly fabricated using LTCC and CMOS processes (e.g., 65-nm CMOS), respectively. The proposed phased array system is expected to be capable of implementing the system at high frequencies, such as Ku or Ka-bands. Because this work focuses on concept proving, a 3.5 GHz 8-element phased array system is opted and built to validate and demonstrate the proposed matrix-sum method. The system presents full beam control with the sum, difference beam pattern, and beam tapering based on comprehensive theoretical derivations.

The remainder of this paper is organized as follows. Section II presents the matrix-sum method and circuit design. Section III introduces the proposed tunable amplifier, a crucial component of the weighting network. Section IV presents a comparative analysis of the proposed phased array system with two other systems in terms of beam angle accuracy and system power budget. Section V describes the experimental setup and presents the obtained results. Finally, Section VI provides the conclusion.

II. MATRIX-SUM METHOD AND CIRCUIT DESIGN

The proposed matrix-sum method can be applied to both the transmitting and receiving modes on the basis of the reciprocity theorem. In this work, an 8-element phased array with transmit mode is selected for demonstration.

Figs. 2 presents the circuit block diagrams of the phased array systems using the matrix-sum method, vector-sum phase shifters, and conventional phase shifters. The proposed phased array system (Fig. 2(a)) comprises a phase matrix network and a weighting network. The input signal (S_{IN}) is fed to the tunable amplifiers, where it is amplified and re-arranged the power ratio at each input signal (a_1 to a_8) of the phase matrix network to generate the desired output signals (b_9 to b_{16}) for synthesizing different beam patterns. Since the power ratio of each

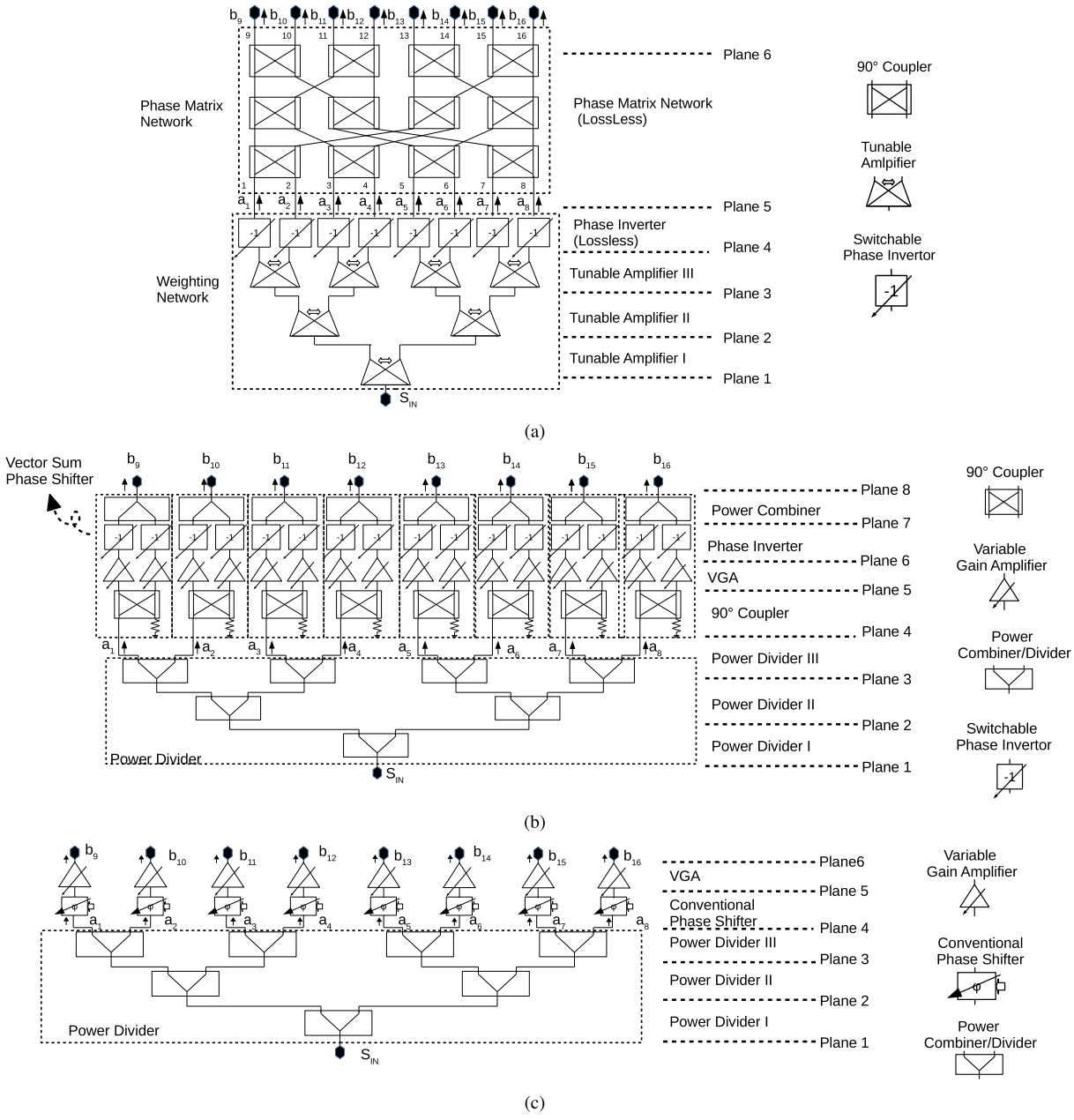

FIGURE 2. **Block diagram of phased array systems using (a) the proposed matrix-sum method, (b) vector-sum phase shifters, and (c) conventional phase shifters.**

path can be adjusted, unnecessary distribution loss can be avoided. Moreover, achieving higher system gain is relatively straightforward because of the use of cascaded tunable amplifiers.

In the phased array system using vector-sum phase shifters (Fig. 2(b)), the input signal (S_{IN}) is fed to the power divider and distributed equally to vector-sum phase shifters to generate the desired output signals for synthesizing the different cases of beam patterns. The architecture of the vector-sum phase shifters involves an unavoidable distribution loss when balancing the output power of each different output phase case. Furthermore, in scenarios involving beam tapering, the equal distribution of the signal to each path results in an unavoidable loss.

In the phased array system (Fig. 2(c)) using conventional phase shifters and magnitude controller (VGA) to form beams. The input signal (S_{IN}) is fed to the power divider; the signal is then distributed equally to the conventional phase shifters and to the VGAs for amplitude weighting in order to generate the desired output signals for synthesizing different beam patterns. Similar to the phased array system using vector-sum phase shifters, the equally distributed to each path results in an unavoidable loss in scenarios involving beam tapering.

In this proposed phased array (Fig. 2(a)), each input signal of the phase matrix network simultaneously inputs to the phase matrix network. The phase matrix is represented based on the definition of generalized scattering matrix (S-parameters), with a_1 to a_8 (incident power waves) being the input signals and b_9 to b_{16} (reflected power waves) being the corresponding output signals [36]. In accordance with the perfect matching condition, signals b_1 to b_8 and a_9 to a_{16} are all zero and the output signals (b_9 to b_{16}) are linear combinations of the input signals (a_1 to a_8), and the transmission coefficients from input ports to output ports are the coefficients of the signals.

Mathematically, the phase matrix network performs the multiplication of the matrix with the vector $[a_1, a_2, \ldots, a_8]^T$ and outputs the signals $[b_9, b_{10}, \ldots, b_{16}]^T$

$$\begin{bmatrix} b_9 \\ b_{10} \\ \vdots \\ b_{16} \end{bmatrix} = M \begin{bmatrix} a_1 \\ a_2 \\ \vdots \\ a_8 \end{bmatrix}. \tag{1}$$

When the target output signals have been determined, the required input signals can be evaluated through an inverse matrix operation

$$\begin{bmatrix} a_1 \\ a_2 \\ \vdots \\ a_8 \end{bmatrix} = M^{-1} \begin{bmatrix} b_9 \\ b_{10} \\ \vdots \\ b_{16} \end{bmatrix}. \tag{2}$$

The evaluated input signals $[a_1, a_2, \ldots, a_8]^T$ can then be rewritten as

$$\begin{bmatrix} a_1 \\ a_2 \\ \vdots \\ a_8 \end{bmatrix} = \begin{bmatrix} |a_1|e^{-j\theta_1} \\ |a_2|e^{-j\theta_2} \\ \vdots \\ |a_8|e^{-j\theta_8} \end{bmatrix} = e^{-j\theta_1} \begin{bmatrix} |a_1|e^{-j(\theta_1-\theta_1)} \\ |a_2|e^{-j(\theta_2-\theta_1)} \\ \vdots \\ |a_8|e^{-j(\theta_8-\theta_1)} \end{bmatrix}. \tag{3}$$

For a given matrix M where $|\theta_n - \theta_1| = 0°$ or $180°$, $n = 1$–8, the input signals $[a_1, a_2, \ldots, a_8]^T$ can be expressed as real numbers

$$\begin{bmatrix} |a_1|e^{-j(\theta_1-\theta_1)} \\ |a_2|e^{-j(\theta_2-\theta_1)} \\ \vdots \\ |a_8|e^{-j(\theta_8-\theta_1)} \end{bmatrix} = \begin{bmatrix} |a_1| \\ (-1)^{i_2}|a_2| \\ \vdots \\ (-1)^{i_8}|a_8| \end{bmatrix} = \begin{bmatrix} R_{a_1} \\ R_{a_2} \\ \vdots \\ R_{a_8} \end{bmatrix}, \tag{4}$$

where i_n is an index that represent whether any of a_2–a_8 is a positive or negative real number, $n = 2$–8. If $i_n = 0$, $|\theta_n - \theta_1| = 0°$, a_n is a positive real number. By contrast, if $i_n = 1$, $|\theta_n - \theta_1| = 180°$, a_n is a negative real number.

Through (2)–(4), the input signal can be converted into a real number signal multiplied by the normalized phase $e^{-j\theta_1}$,

$$\begin{bmatrix} a_1 \\ a_2 \\ \vdots \\ a_8 \end{bmatrix} = e^{-j\theta_1} \begin{bmatrix} R_{a_1} \\ R_{a_2} \\ \vdots \\ R_{a_8} \end{bmatrix} = M^{-1} \begin{bmatrix} b_9 \\ b_{10} \\ \vdots \\ b_{16} \end{bmatrix}. \tag{5}$$

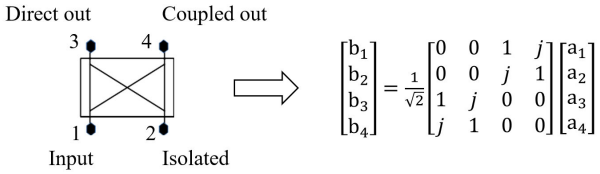

FIGURE 3. Block diagram of the 90° coupler.

By multiplying both sides of (1) by $e^{j\theta_1}$, (2) can be rewritten as

$$e^{j\theta_1} \begin{bmatrix} b_9 \\ b_{10} \\ \vdots \\ b_{16} \end{bmatrix} = M \begin{bmatrix} R_{a_1} \\ R_{a_2} \\ \vdots \\ R_{a_8} \end{bmatrix}. \tag{6}$$

Because $e^{j\theta_1}$ is a constant, the pattern of the output signals $e^{j\theta_1}[b_9, b_{10}, \ldots, b_{16}]^T$ is identical to that of the output signals $[b_9, b_{10}, \ldots, b_{16}]^T$. Moreover, because $[R_{a_1}, R_{a_2}, \ldots, R_{a_8}]^T$ are all real numbers, they can be generated by the circuit using power division, magnitude weighting, and sign switching functions. Similar to the benefits of vector-sum phase shifters, the complex-number-operation functions (phase shifting) are replaced by real-number-operation functions (magnitude weighting and sign switching). For the response speed, although the proposed method may need more computation resources for establishing the beam table, it has the same response time compared to the other two methods as the beam table established.

Notably, (6) is a special case. An arbitrary phase matrix network (M) does not have the property that the phase difference between the evaluated input signals a_1–a_8 from (2) are either 0° or 180°. Therefore, it is crucial to find a feasible phase matrix network. A feasible phase matrix network is shown in Fig. 2(a). This 8 × 8 phase matrix network comprises twelve 90° hybrid couplers. According to the S-parameters of a 90° hybrid coupler (shown in Fig. 3) [36], the relation between output signals (b_3 and b_4) and input signals (a_1 and a_2) is derived as

$$\begin{aligned} b_3 &= a_1 S_{31} + a_2 S_{32} \\ b_4 &= a_1 S_{41} + a_2 S_{42}. \end{aligned} \tag{7}$$

Then phase matrix (M) of a 90° hybrid coupler can be derived according to (7) as follow

$$\begin{bmatrix} b_3 \\ b_4 \end{bmatrix} = M \begin{bmatrix} a_1 \\ a_2 \end{bmatrix} = \frac{1}{\sqrt{2}} \begin{bmatrix} e^{j0} & e^{-j\frac{\pi}{2}} \\ e^{-j\frac{\pi}{2}} & e^{j0} \end{bmatrix} \begin{bmatrix} a_1 \\ a_2 \end{bmatrix}, \tag{8}$$

Similarly, the phase matrix M of the 8 × 8 novel phase matrix network can be derived by evaluating the S-parameters and determining the relation between the output signals and

the input signals

$$M = L_{\mathrm{PMN}} \times e^{-j\alpha} \times \begin{bmatrix} e^{j0} & e^{-j\frac{\pi}{2}} & e^{-j\frac{\pi}{2}} & e^{-j\pi} & e^{-j\frac{\pi}{2}} & e^{-j\pi} & e^{-j\pi} & e^{j\frac{\pi}{2}} \\ e^{-j\frac{\pi}{2}} & e^{-j\pi} & e^{-j\pi} & e^{j\frac{\pi}{2}} & e^{j0} & e^{-j\frac{\pi}{2}} & e^{-j\frac{\pi}{2}} & e^{-j\pi} \\ e^{-j\frac{\pi}{2}} & e^{-j\pi} & e^{j0} & e^{-j\frac{\pi}{2}} & e^{-j\pi} & e^{j\frac{\pi}{2}} & e^{-j\frac{\pi}{2}} & e^{-j\pi} \\ e^{-j\pi} & e^{j\frac{\pi}{2}} & e^{-j\frac{\pi}{2}} & e^{-j\pi} & e^{-j\frac{\pi}{2}} & e^{-j\pi} & e^{j0} & e^{-j\frac{\pi}{2}} \\ e^{-j\frac{\pi}{2}} & e^{j0} & e^{-j\pi} & e^{-j\frac{\pi}{2}} & e^{-j\pi} & e^{-j\frac{\pi}{2}} & e^{j\frac{\pi}{2}} & e^{-j\pi} \\ e^{-j\pi} & e^{-j\frac{\pi}{2}} & e^{j\frac{\pi}{2}} & e^{-j\pi} & e^{-j\frac{\pi}{2}} & e^{j0} & e^{-j\pi} & e^{-j\frac{\pi}{2}} \\ e^{-j\pi} & e^{-j\frac{\pi}{2}} & e^{-j\frac{\pi}{2}} & e^{j0} & e^{j\frac{\pi}{2}} & e^{-j\pi} & e^{-j\pi} & e^{-j\frac{\pi}{2}} \\ e^{j\frac{\pi}{2}} & e^{-j\pi} & e^{-j\pi} & e^{-j\frac{\pi}{2}} & e^{-j\pi} & e^{-j\frac{\pi}{2}} & e^{-j\frac{\pi}{2}} & e^{j0} \end{bmatrix}, \tag{9}$$

where L_{PMN} is the distribution and transmission loss. If all the components are lossless, L_{PMN} is equal to $\frac{1}{\sqrt{2}}$ cubed; that is, $\frac{1}{\sqrt{8}}$. $e^{-j\alpha}$ is the phase delay of the shortest path in the phase matrix network if the phase network contains an additional interconnection transmission line.

Suppose that the output is set to synthesize a sum (normal) 8-element antenna beam pattern with a given beam angle, the related output signals b_9–b_{16} can be expressed as

$$\begin{bmatrix} b_9 \\ b_{10} \\ b_{11} \\ b_{12} \\ b_{13} \\ b_{14} \\ b_{15} \\ b_{16} \end{bmatrix} = k \begin{bmatrix} e^{-j0\phi} \\ e^{-j1\phi} \\ e^{-j2\phi} \\ e^{-j3\phi} \\ e^{-j4\phi} \\ e^{-j5\phi} \\ e^{-j6\phi} \\ e^{-j7\phi} \end{bmatrix}, \tag{10}$$

where k represents the amplitude of the output signals b_9-b_{16} and ϕ is calculated using the beam angle (θ_d)

$$\phi = \frac{2\pi d \sin\theta_d}{\lambda}, \tag{11}$$

where d is the antenna spacing and is assumed to be half wavelength in general.

Applying (2), (9), (10), and (11) can yield the input signals a_1–a_8 as follows

$$\begin{aligned} a_1 &= |a_1|e^{-j\theta_1} = \frac{k\cdot e^{j\alpha}}{8L_{PMN}}(A_1 + jB_1) \\ A_1 &= 1 + \sin\phi + \sin 2\phi - \cos 3\phi \\ &\quad + \sin 4\phi - \cos 5\phi - \cos 6\phi - \sin 7\phi \\ B_1 &= \cos\phi + \cos 2\phi + \sin 3\phi \\ &\quad + \cos 4\phi + \sin 5\phi + \sin 6\phi - \cos 7\phi \end{aligned} \tag{12}$$

$$\begin{aligned} a_2 &= |a_2|e^{-j\theta_2} = \frac{k\cdot e^{j\alpha}}{8L_{PMN}}(A_2 + jB_2) \\ A_2 &= -\cos\phi - \cos 2\phi - \sin 3\phi \\ &\quad + \cos 4\phi + \sin 5\phi + \sin 6\phi - \cos 7\phi \\ B_2 &= 1 + \sin\phi + \sin 2\phi - \cos 3\phi \\ &\quad - \sin 4\phi + \cos 5\phi + \cos 6\phi + \sin 7\phi \end{aligned} \tag{13}$$

$$\begin{aligned} a_3 &= |a_3|e^{-j\theta_3} = \frac{k\cdot e^{j\alpha}}{8L_{PMN}}(A_3 + jB_3) \\ A_3 &= -\cos\phi + \cos 2\phi + \sin 3\phi \\ &\quad - \cos 4\phi - \sin 5\phi + \sin 6\phi - \cos 7\phi \\ B_3 &= 1 + \sin\phi - \sin 2\phi + \cos 3\phi \\ &\quad + \sin 4\phi - \cos 5\phi + \cos 6\phi + \sin 7\phi \end{aligned} \tag{14}$$

$$\begin{aligned} a_4 &= |a_4|e^{-j\theta_4} = \frac{k\cdot e^{j\alpha}}{8L_{PMN}}(A_4 + jB_4) \\ A_4 &= -1 - \sin\phi + \sin 2\phi - \cos 3\phi \\ &\quad + \sin 4\phi - \cos 5\phi + \cos 6\phi + \sin 7\phi \\ B_4 &= -\cos\phi + \cos 2\phi + \sin 3\phi \\ &\quad + \cos 4\phi + \sin 5\phi - \sin 6\phi + \cos 7\phi \end{aligned} \tag{15}$$

$$\begin{aligned} a_5 &= |a_5|e^{-j\theta_5} = \frac{k\cdot e^{j\alpha}}{8L_{PMN}}(A_5 + jB_5) \\ A_5 &= \cos\phi - \cos 2\phi + \sin 3\phi \\ &\quad - \cos 4\phi + \sin 5\phi - \sin 6\phi - \cos 7\phi \\ B_5 &= 1 - \sin\phi + \sin 2\phi + \cos 3\phi \\ &\quad + \sin 4\phi + \cos 5\phi - \cos 6\phi + \sin 7\phi \end{aligned} \tag{16}$$

$$\begin{aligned} a_6 &= |a_6|e^{-j\theta_6} = \frac{k\cdot e^{j\alpha}}{8L_{PMN}}(A_6 + jB_6) \\ A_6 &= -1 + \sin\phi - \sin 2\phi - \cos 3\phi \\ &\quad + \sin 4\phi + \cos 5\phi - \cos 6\phi + \sin 7\phi \\ B_6 &= \cos\phi - \cos 2\phi + \sin 3\phi \\ &\quad + \cos 4\phi - \sin 5\phi + \sin 6\phi + \cos 7\phi \end{aligned} \tag{17}$$

$$\begin{aligned} a_7 &= |a_7|e^{-j\theta_7} = \frac{k\cdot e^{j\alpha}}{8L_{PMN}}(A_7 + jB_7) \\ A_7 &= -1 + \sin\phi + \sin 2\phi + \cos 3\phi \\ &\quad - \sin 4\phi - \cos 5\phi - \cos 6\phi + \sin 7\phi \\ B_7 &= \cos\phi + \cos 2\phi - \sin 3\phi \\ &\quad - \cos 4\phi + \sin 5\phi + \sin 6\phi + \cos 7\phi \end{aligned} \tag{18}$$

$$\begin{aligned} a_8 &= |a_8|e^{-j\theta_8} = \frac{k\cdot e^{j\alpha}}{8L_{PMN}}(A_8 + jB_8) \\ A_8 &= -\cos\phi - \cos 2\phi + \sin 3\phi \\ &\quad - \cos 4\phi + \sin 5\phi + \sin 6\phi + \cos 7\phi \\ B_8 &= -1 + \sin\phi + \sin 2\phi + \cos 3\phi \\ &\quad + \sin 4\phi + \cos 5\phi + \cos 6\phi - \sin 7\phi \end{aligned} \tag{19}$$

The phase difference between any pair of a_1 to a_8 is 0° or 180°. This can be verified by treating the complex values $A_m + jB_m, A_n + jB_n$ as two vectors (A_m, B_m) and (A_n, B_n) on a 2D Cartesian coordinate system and evaluating the absolute value of the cross products of these two vectors

$$|(A_m, B_m) \times (A_n, B_n)| = |(B_m A_n) - (A_m B_n)|, \tag{20}$$

where $m, n = 1$–8 and $m \neq n$. If $|(A_m, B_m) \times (A_n, B_n)|$ is zero, the relative phase difference between any of the calculated a_1–a_8 is either 0° or 180°.

(12) to (19) and (20) indicate that, for a given ϕ, a solution (a_1–a_8) exists and are all real numbers. These findings suggest that the output signals of the proposed 8 × 8 phase matrix

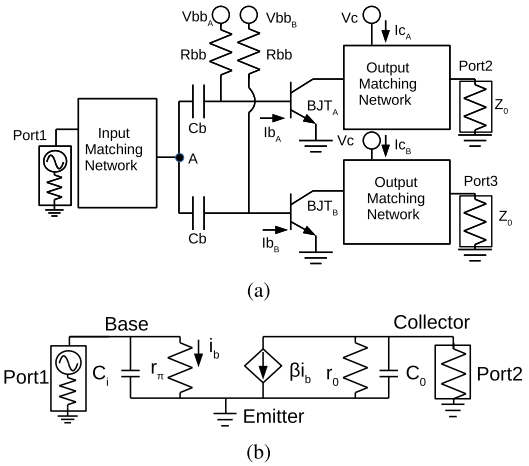

FIGURE 4. Proposed tunable amplifier: (a) schematic diagram and (b) equivalent circuit of the BJT used in the architecture.

network can synthesize a specified phase difference with only real number weightings.

This proposed method can not only form sum beam patterns but also form difference beam patterns and variable beam-width patterns. For the difference beam pattern, the output signals b_9–b_{16} are defined as

$$\begin{bmatrix} b_9 \\ b_{10} \\ b_{11} \\ b_{12} \\ b_{13} \\ b_{14} \\ b_{15} \\ b_{16} \end{bmatrix} = k \begin{bmatrix} 1 \times e^{-j0\phi} \\ 1 \times e^{-j1\phi} \\ 1 \times e^{-j2\phi} \\ 1 \times e^{-j3\phi} \\ -1 \times e^{-j4\phi} \\ -1 \times e^{-j5\phi} \\ -1 \times e^{-j6\phi} \\ -1 \times e^{-j7\phi} \end{bmatrix}. \tag{21}$$

Furthermore, for the sum pattern with variable beam-width, the output signals b_9–b_{16} can be defined by non-uniform weighting as

$$\begin{bmatrix} b_9 \\ b_{10} \\ b_{11} \\ b_{12} \\ b_{13} \\ b_{14} \\ b_{15} \\ b_{16} \end{bmatrix} = k \begin{bmatrix} m_1 \times e^{-j0\phi} \\ m_2 \times e^{-j1\phi} \\ m_3 \times e^{-j2\phi} \\ m_4 \times e^{-j3\phi} \\ m_4 \times e^{-j4\phi} \\ m_3 \times e^{-j5\phi} \\ m_2 \times e^{-j6\phi} \\ m_1 \times e^{-j7\phi} \end{bmatrix}, \tag{22}$$

where m_1–m_4 are the ratios of the magnitudes. It is noteworthy that reducing the antenna weights (m_1 and m_2) towards the side positions leads to increased beam-width, akin to synthesizing the beam with fewer antennas. On the basis of the derived steps ((12)–(19)), the required weighting can be determined and verified to be a set of real numbers. The detailed derivations are provided in Appendix. Experiment examples of the sum (10), difference (21), and variable beam-with (22) patterns are presented in Section V.

III. TUNABLE AMPLIFIER

The schematic of the proposed 1-to-2 tunable amplifier is shown in Fig. 4(a). Two bipolar junction transistors (BJT), labeled as BJT_A and BJT_B, are biased using large capacitors (Cb) and resistors (Rbb). The value of Cb and Rbb is large enough to ensure that these components function only as a biasing network and can be omitted in the RF small-signal analysis. The base currents (Ib_A and Ib_B) can be controlled independently. The input nodes of the two BJTs are connected at node A. An input matching network is applied to match the impedance of the shunted BJTs to the system impedance. Two identical output matching networks are applied to the output ports of BJTs to match the output impedance of the BJTs to the system impedance (Z_0). The output matching networks provide the biasing currents (Ic_A and Ic_B) of the BJTs.

Fig. 4(b) shows the small-signal equivalent circuit of BJT used for this analysis. The capacitance effects are equivalent to C_i and C_o at the base and collector nodes, respectively. Considering the input resistance (r_π), output resistance (r_0), and current gain (β), the gain of a BJT with conjugate matched source/load impedance ($G_{BJT,M}$) can be derived as

$$G_{BJT,M} = -\frac{\beta}{2}\sqrt{\frac{r_0}{r_\pi}}. \tag{23}$$

On the basis of the relationship between the parameters and the bias ($r_\pi = \beta V_T/Ic$, $Ic = \beta Ib$), $G_{BJT,M}$ can be derived as

$$G_{BJT,M} = -\frac{1}{2}\sqrt{\frac{\beta r_0}{V_T}}\sqrt{Ic}. \tag{24}$$

A small-signal model of the proposed 1-to-2 tunable amplifier is illustrated in Fig. 5. This model indicates that the input resonated capacitance can be merged into input/output matching networks as source/load networks because the input node of the two BJTs (i.e., BJT_A and BJT_B) are shunt connected. Thus, the circuit is simplified as two current control sources connected with one source network and two load networks. $S_{21,M}$ and $S_{31,M}$ can be derived as follows, respectively, under simultaneous conjugate matching conditions

$$\begin{aligned} S_{21,M} &= -\frac{\beta}{2}\sqrt{\frac{r_0}{r_{\pi A}//r_{\pi B}}}\frac{r_{\pi B}}{r_{\pi A}+r_{\pi B}} \\ &= -\frac{1}{2}\sqrt{\frac{\beta r_0}{V_T}}\frac{Ic_A}{\sqrt{Ic_A+Ic_B}}, \end{aligned} \tag{25}$$

$$\begin{aligned} S_{31,M} &= -\frac{\beta}{2}\sqrt{\frac{r_0}{r_{\pi A}//r_{\pi B}}}\frac{r_{\pi A}}{r_{\pi A}+r_{\pi B}} \\ &= -\frac{1}{2}\sqrt{\frac{\beta r_0}{V_T}}\frac{Ic_B}{\sqrt{Ic_A+Ic_B}}. \end{aligned} \tag{26}$$

According to (25) and (26), the ratio between $S_{21,M}$ and $S_{31,M}$ can be obtained as the ratio of Ic_A and Ic_B as

$$\frac{S_{31,M}}{S_{21,M}} = \frac{Ic_B}{Ic_A}. \tag{27}$$

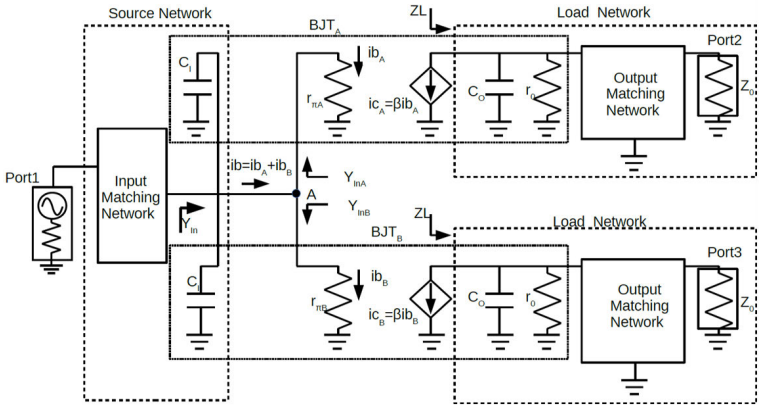

FIGURE 5. Small-signal model of the proposed 1-to-2 tunable amplifier.

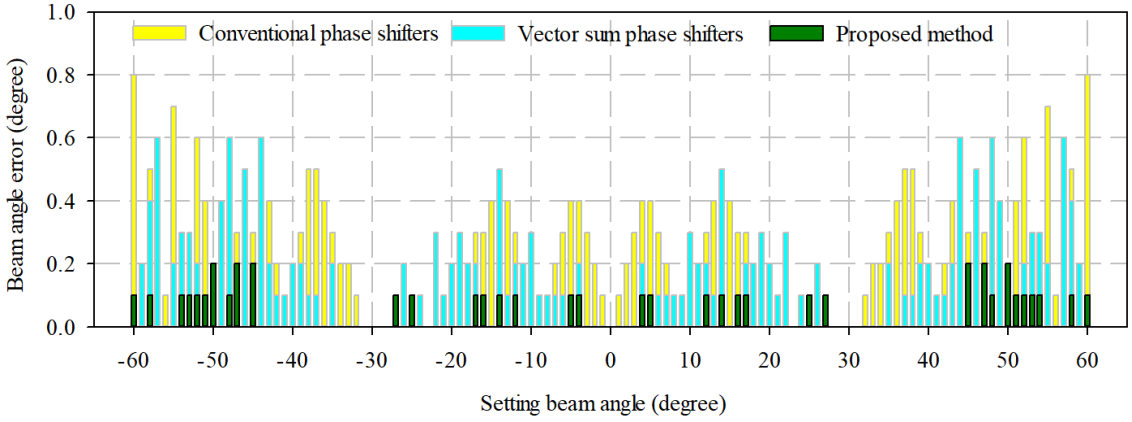

FIGURE 6. Beam angle error comparison with a beam angle step of 1°.

Regarding the matching condition, r_0 of the BJT does not change significantly in this work. Therefore, the output matching condition does not change during the tuning $\mathrm{Ic_A}$ and $\mathrm{Ic_B}$. For the input matching condition, the input admittance Y_{in} must be considered because the input admittance is related to the biasing condition as

$$Y_{\mathrm{in}} = Y_{\mathrm{inA}} + Y_{\mathrm{inB}} = \frac{1}{r_{\pi \mathrm{A}} // r_{\pi \mathrm{B}}} = \frac{\mathrm{Ic_A} + \mathrm{Ic_B}}{\beta \mathrm{V_T}}. \tag{28}$$

According to (28), the summation of $\mathrm{Ic_A}$ and $\mathrm{Ic_B}$ determines the input admittance. Since the matching networks are fixed during the tuning of $S_{31,M}$ and $S_{21,M}$, $\mathrm{Ic_A} + \mathrm{Ic_B}$ must be selected to have low reflection coefficients.

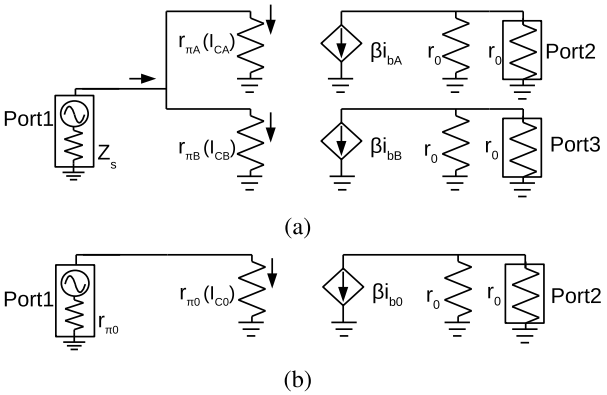

FIGURE 7. Simplified schematic of (a) the tunable amplifier and (b) single BJT.

IV. DISCUSSION OF BEAM ANGLE ACCURACY AND SYSTEM POWER BUDGET

This section discusses two important benefits of the phased array system: beam angle accuracy and system power budget. All discussions are under the same calculated situation of components that have the same total gain, loss, and zero phase and amplitude error.

A. BEAM ANGLE ACCURACY

The phased array systems illustrated in Figs. 2 are digitally controlled; thus, the control step of phase and amplitude will impact the synthesized pattern. In this study, the beam angle accuracy was determined by calculating the difference

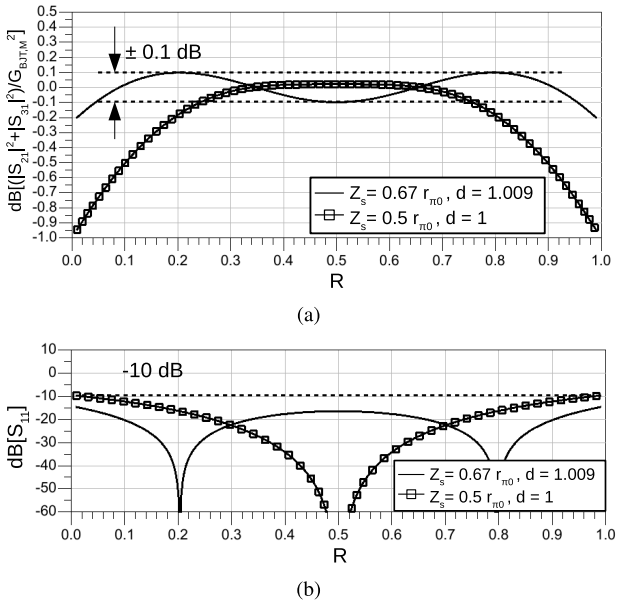

FIGURE 8. Optimal results of the proposed tunable amplifier: (a) power discrepancy and (b) input reflection coefficients.

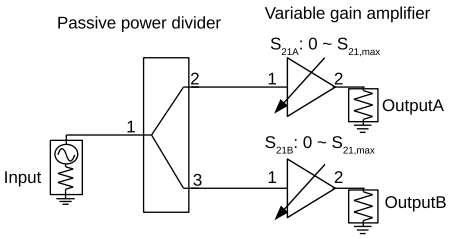

FIGURE 9. Conventional 1-to-2 magnitude controller.

between the beam angle produced by each of the phased array systems in Figs. 2 with that produced by the phased array systems ideally calculated with the output signal phase ϕ in (11). In this analysis, the passive components (90° couplers, switchable phase inverters, and power combiner/dividers) are assumed to be ideal components; thus, the calculated beam angle errors were those caused by only the control resolution. In this case, a 7-bit control resolution was selected. For a fair comparison, the weighting for both vector-sum phase shifters and the proposed method was a 1-bit phase inverter and a 6-bit amplitude controller with the smallest amplitude step of 0.5 dB. The beam angle errors for the three methods were calculated among the commonly used beam angle range of −60° to 60° with a 1° step and the results are displayed in Fig. 6.

These results demonstrated that the phased array system with the conventional phase shifters has the highest beam angle error (0.8°), whereas the phased array system with the proposed method has the lowest beam angle error (0.2°). Hence, the array system with the proposed method can achieve more accurate beam angles than the other two systems, suggesting that it could achieve the same beam accuracy as other methods with fewer control bits. Therefore, the proposed method offers advantages in system design for the same beam angle accuracy.

B. SYSTEM POWER BUDGET

Because a phased array system is a 1-to-N network, the S-parameters of one transverse path (S_{MN}, $M \neq N$) cannot represent the power budget of the system. Therefore, the system power budget is determined by the total power of the signals in the reference planes in this work. According to Fig. 2(a), the proposed system contains six reference planes. The input signal S_{IN} is injected to Plane 1, and the weighting network distributes and weights the input signal S_{IN} as a_1–a_8 on Plane 5; these weighted signals are redistributed by the phase matrix network as the output signals (b_9–b_{16}) to Plane 6. If the phase inverters are assumed to be lossless, the total power into Plane 4 is equal to the total power into Plane 5. Because the phase matrix network is ideally lossless and passive, the power conservation property between the input (a_1–a_8) and output signals (b_9–b_{16}) is valid

$$\sum_{n=1}^{8} |a_n|^2 = \sum_{n=9}^{16} |b_n|^2. \tag{29}$$

Therefore, the system power budget is dominated by the 1-to-2 tunable amplifiers (Tunable Amplifier I, Tunable Amplifier II, and Tunable Amplifier III). According to (25) and (26), the ratio between the input and output power can be evaluated as

$$|S_{21,M}|^2 + |S_{31,M}|^2 = \frac{1}{4}\frac{\beta r_0}{V_T}\frac{Ic_A{}^2 + Ic_B{}^2}{Ic_A + Ic_B}. \tag{30}$$

The sum of Ic_A and Ic_B, as well as that of $Ic_A{}^2$ and $Ic_B{}^2$ determine the output power. During the tuning of weights, (28) and (30) must be considered to optimize the performance of the tunable amplifiers for the system power budget.

Figs. 7 presents a simplified schematic of the proposed tunable amplifier and a single BJT. Because the reactance of BJTs will be resonated with matching networks, the reactance can be disregarded in this discussion. In Fig. 7(a), the source impedance of the tunable amplifier is set to Z_s. $r_{\pi A}$ and $r_{\pi B}$ are functions of Ic_A and Ic_B, respectively. By introducing the collector current (I_C) of a BJT in (24), (30) can be rewrite as

$$\begin{aligned}\frac{1}{4}\frac{\beta r_0}{V_T}\frac{Ic_A{}^2 + Ic_B{}^2}{Ic_A + Ic_B} &= \frac{1}{4}\frac{\beta r_0 (Ic_A + Ic_B)}{V_T}\frac{Ic_A{}^2 + Ic_B{}^2}{(Ic_A + Ic_B)^2} \\ &= \frac{1}{4}\frac{\beta r_0 I_C}{V_T}\frac{Ic_A + Ic_B}{I_C}\left[\left(\frac{Ic_A}{Ic_A + Ic_B}\right)^2 \right. \\ &\quad \left. + \left(1 - \left(\frac{Ic_A}{Ic_A + Ic_B}\right)^2\right)\right]. \end{aligned} \tag{31}$$

Let factor (R) be the ratio of Ic_A to $Ic_A + Ic_B$, and the factor (F) be the ratio of $Ic_A + Ic_B$ to I_C. Accordingly, the ratio between the total output power and the input power can be evaluated as

$$|S_{21,M}|^2 + |S_{31,M}|^2 = \frac{1}{4}\frac{\beta r_0 I_C}{V_T} F((R^2) + (1 - R)^2). \tag{32}$$

TABLE 1. System loss comparison of the 8-element phased array topology that uses three different methods with different cases.

Method	System loss(dB)			
	Case1	Case2	Case3	Case4
Conventional phase shifters	0	0	3	6
Vector-sum phase shifters	6	6	9	12
Proposed matrix-sum method	**0**	**0**	**0**	**0**

Case1: Sum beam pattern setting.
Case2: Difference beam pattern setting.
Case3: Beam-width control with output amplitude ratio (0:0:1:1:1:1:0:0).
Case4: Beam-width control with output amplitude ratio (0:0:0:1:1:0:0:0).

As indicated in (27), the ratio between $|S_{21,M}|$ and $|S_{31,M}|$ can be controlled by changing the ratio between $\mathrm{Ic_A}$ and $\mathrm{Ic_B}$. Therefore, the factor F also changes with the ratio. However, the total output power of the two ports must not be changed when changing F. According to (32), F must be adjusted with respect to R to maintain the total power. To ensure that $|S_{21,M}|^2+|S_{31,M}|^2$ is unchanged, F can be selected as follow

$$F = \mathrm{d}/(\mathrm{R}^2 + (1-\mathrm{R})^2)), \tag{33}$$

where d is a tuning factor of F. However, the input admittance will change while tuning F (28). Therefore, the source impedance $\mathrm{Z_s}$ must be adjusted to ensure that the input reflection coefficient is smaller than -10 dB. Adjusting d and $\mathrm{Z_s}$ can yield an optimal solution that meets the approximate condition

$$|S_{21,M}|^2 + |S_{31,M}|^2 \simeq |\mathrm{G_{BJT,M}}|^2. \tag{34}$$

Herein, we consider two cases: in the first case, $\mathrm{Z_s} = 0.5\mathrm{r}_{\pi 0}$, d = 1; in the second case, $\mathrm{Z_s} = 0.67\mathrm{r}_{\pi 0}$, d = 1.009. In the first case, both $|S_{21,M}|^2 + |S_{31,M}|^2$ and the reflection coefficient can be optimized if the power is equally split (R = 0.5). However, if the power ratio is not equally split and R is close to 0 or 1, the input impedance is not matched to the source impedance. Thus, the output power is degraded. Therefore, in the second case, $\mathrm{Z_s}$ and d are fine-tuned to achieve a balance between the variance of output power and the performance of the reflection coefficient, respectively. Figs. 8 indicates that the transmission coefficient in the first case degraded such that there is 0.95 dB loss while R is close to 0 or 1. In the second case, the output power is maintained in the range of ±0.1 dB while R is between 0.05 to 0.95. Therefore, by setting Zs and d to the second case, the tunable amplifier can be considered equivalent to an ideal power divider with power conservation properties and an amplifier with a maximum S_{21}.

A conventional tunable amplifier can be realized using a 1-to-2 passive power divider and VGAs, as shown in Fig. 9. Let the maximum S_{21} of the VGA be $S_{21,\max}$. The maximum gain from the input port to each output port is then $\frac{S_{21,\max}}{\sqrt{2}}$ because S_{21} and S_{31} of a passive power divider are ideally $\frac{1}{\sqrt{2}}$.

If an incident power wave ($1e^{j0}$) is input to port 1 of the power divider, the output signals of OutputA and OutputB ports are $\frac{S_{21\mathrm{A}}}{\sqrt{2}}$ and $\frac{S_{21\mathrm{B}}}{\sqrt{2}}$, respectively. If both VGAs are operated at maximum gain, the total output power is $|\frac{S_{21\mathrm{A}}}{\sqrt{2}}|^2 + |\frac{S_{21\mathrm{B}}}{\sqrt{2}}|^2 = |\frac{S_{21,\max}e^{j0}}{\sqrt{2}}|^2 + |\frac{S_{21,\max}e^{j0}}{\sqrt{2}}|^2 = |S_{21,\max}|^2$. In other words, the input power is equally split and amplified with a gain of $S_{21,\max}$. However, if one of the amplifiers is set to zero gain ($S_{21} = 0$), the total power becomes $|\frac{S_{21,\max}e^{j0}}{\sqrt{2}}|^2 + 0 = \frac{|S_{21,\max}|^2}{2}$. In view of power conservation, half of the power is lost in the power divider. Therefore, in a conventional tunable amplifier, power loss is inevitable due to varying weighting factors. In the most extreme case, the total power will have a 3 dB loss. A conventional 8-way tunable amplifier has a 1-to-8 power divider; therefore, the maximum power loss is 9 dB. Specifically, the system power budget of the proposed system can be improved by 9 dB by using the proposed tunable amplifier instead of the conventional tunable amplifier.

To fully discuss the comparison of the power budgets of the systems in Figs. 2, two scenarios are considered for discussion. The first scenario involves equal signal magnitudes at each output port ($\mathrm{B_1}$–$\mathrm{B_8}$) for beam steering; the second scenario has set the output signals to have different magnitudes for beam-width control. For simplicity, the connections of the components can be assumed to be perfectly matched, and the loss of the passive components (power divider/combiners, switchable phase inverters, 90° couplers, and conventional phase shifters) can be assumed to be equal to zero.

In the first scenario, the total power on the output plane (Plane 6) of the proposed system (Fig. 2(a)) is equal to the total output power of the tunable amplifier III on Plane 4; this is because the phase matrix network and phase inverters are assumed to be lossless. For the tunable amplifier designed according to (33), the total power is identical to the input power of $\mathrm{S_{IN}}$ in a three-stage amplifier

$$\sum_{n=9}^{16} |\mathrm{b}_n|^2 = \sum_{n=1}^{8} |\mathrm{a}_n|^2 = |\mathrm{G_{BJT,M}}|^2 |\mathrm{G_{BJT,M}}|^2 |\mathrm{G_{BJT,M}}|^2 |\mathrm{S_{IN}}|^2. \tag{35}$$

For the phased array using vector-sum phase shifters (Fig. 2(b)), the power input to Plane 1 is identical to the total power output from Plane 4. The output power of the phased array can be expressed as

$$\sum_{n=1}^{8} |\mathrm{B}_n|^2 = |\mathrm{G_{VSPS,M}}|^2 |\mathrm{S_{IN}}|^2, \tag{36}$$

where $\mathrm{G_{VSPS,M}}$ is the gain of the vector-sum phase shifter and can be expressed as

$$\mathrm{G_{VSPS,M}} = \frac{1}{\sqrt{2}}(G_a + jG_b)\frac{1}{\sqrt{2}}, \tag{37}$$

where G_a and G_b are the gain of the VGA and the phase inverter. G_a and G_b must be tuned to synthesize the desired phase shift. If one of G_a or G_b is zero and the other amplifier

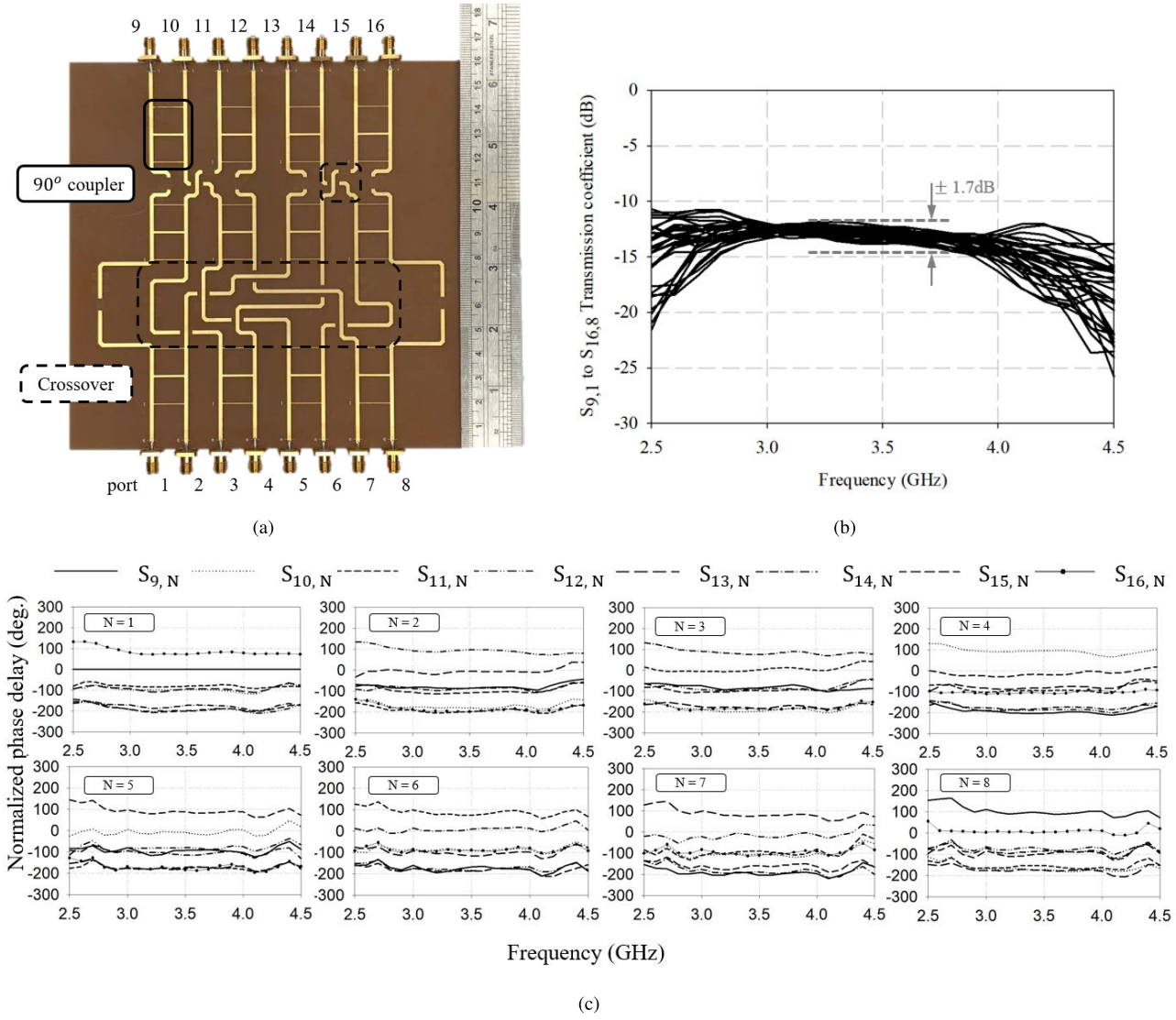

FIGURE 10. Proposed 8 × 8 phase matrix network: (a) circuit photograph of the fabricated prototype, (b) measured transmission coefficient, and (c) normalized phase delay.

is set to be the maximum gain of a VGA ($G_{VGA,M}$), the gain of a vector-sum phase shifter can be derived as

$$|G_{VSPS,M}|^2 = \frac{1}{2}|G_{VGA,M}|^2\frac{1}{2} = \frac{1}{4}|G_{VGA,M}|^2, \tag{38}$$

and the output power of the phased array can be derived as

$$\sum_{n=9}^{16}|b_n|^2 = \frac{1}{4}|G_{VGA,M}|^2|S_{IN}|^2. \tag{39}$$

For the phased array using conventional phase shifters (Fig. 2(c)), because the conventional phase shifter is assumed to be lossless, the total output power of the phased array can be expressed as

$$\sum_{n=9}^{16}|b_n|^2 = |G_{VGA,M}|^2|S_{IN}|^2. \tag{40}$$

By observing (35), (39), and (40), the proposed phased array system has the highest total power.

Select the VGA to be the same stage number of the tunable amplifier in these two phased array systems ($|G_{VGA,M}| = |G_{BJT,M}||G_{BJT,M}||G_{BJT,M}|$). The total power of the phased array system in Fig. 2(c) can then be equal to that of the proposed phased array system. However, the phased array system using vector-sum phase shifter (Fig. 2(b)) still has an unavoidable 1/4 power loss (6 dB).

For the second scenario, in which output signals have different magnitudes for beam-width control, the proposed phased array system can simultaneously control the amplitude and phase at each output port on Plane 6; therefore, the total power relationship between the output and input signals is unchanged, as indicated in (35). For the other phased array systems (Figs. 2(b) and (c)), the input signal(S_{IN}) is equally

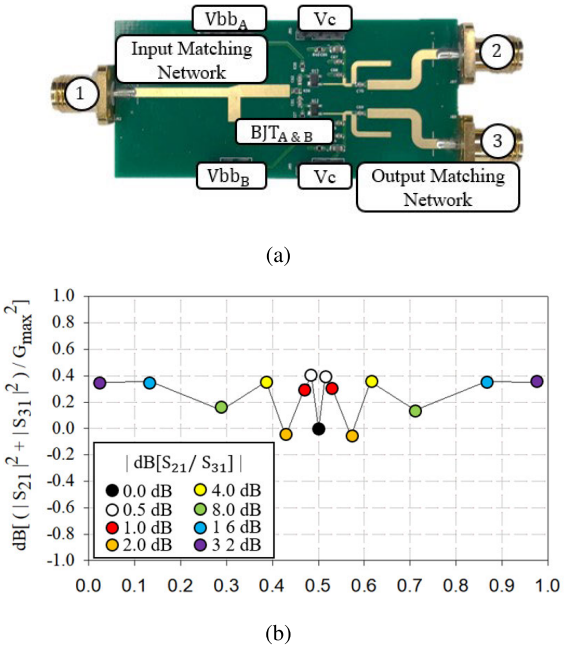

FIGURE 11. Proposed 1-to-2 tunable amplifier: (a) circuit photograph of the fabricated prototype and (b) normalized power sum measurements at different R settings (power differences of 0.5 dB per step) at 3.5 GHz.

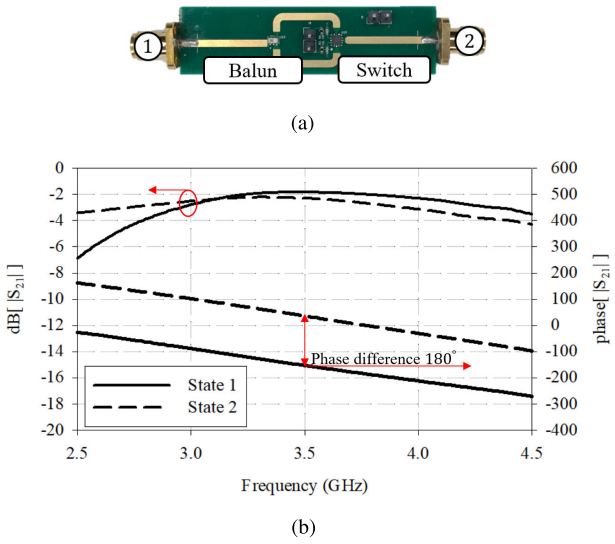

FIGURE 12. Proposed switchable phase inverter: (a) circuit photograph of the fabricated prototype and (b) measured magnitudes and phases of two states.

distributed to Plane 4, assuming each channel has a different gain setting to final Plane 6 (Fig. 2(b)) and Plane8 (Fig. 2(c)), the total output power can be derived as

$$\sum_{n=9}^{16}|b_n|^2=(\sum_{n=1}^{8}(\frac{1}{2})^3|G_{CH,n}|^2)|S_{IN}|^2=\frac{1}{8}(\sum_{n=1}^{8}|G_{CH,n}|^2)|S_{IN}|^2, \tag{41}$$

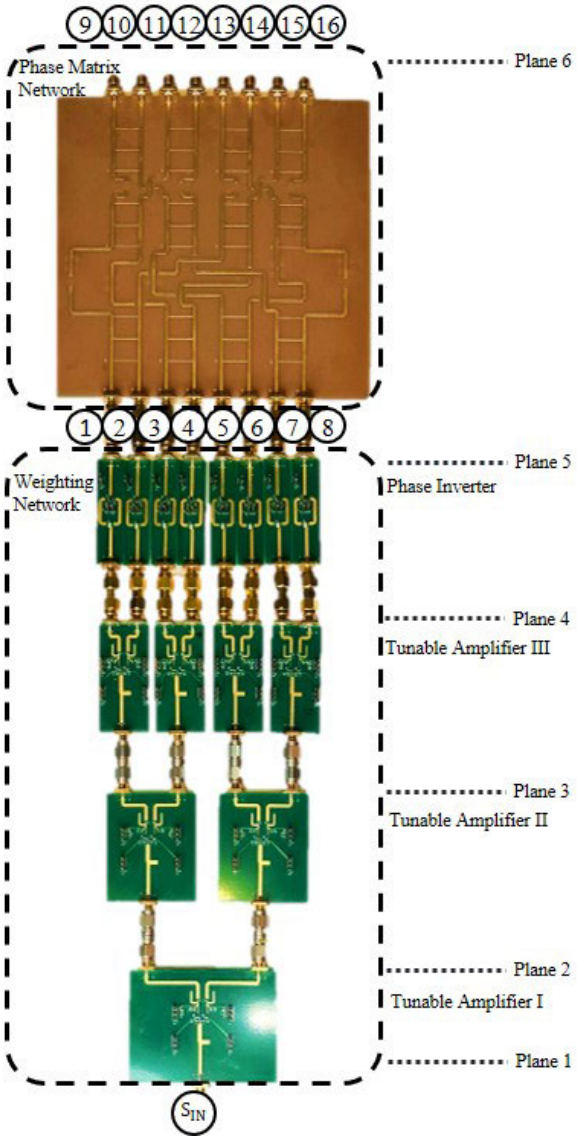

FIGURE 13. Proposed 8-element phased array system circuit photo.

where $G_{CH,n}$ is the final output gain of each channel of the phased array system using conventional phase shifters ($G_{VGA,n}$) or using vector-sum phase shifters ($G_{VSPS,n}$).

Because the channels have unequal power, the total power in (42) is lower than that in (35). For example, the ratio of the final output gain of each channel is (0:0:1:1:1:1:0:0); only four terms contribute to the total output power

$$\sum_{n=9}^{16}|b_n|^2=\frac{1}{8}(\sum_{n=3}^{6}|G_{CH,n}|^2)|S_{IN}|^2=\frac{1}{2}|G_{CH,M}|^2|S_{IN}|^2, \tag{42}$$

where $G_{CH,M}$ is the maximum gain of each channel.

According to (42), the output power of the second scenario will be at least 1/2 (-3 dB) lower than that in the first scenario. For the system using vector-sum phase shifters, $G_{CH,M}$ is

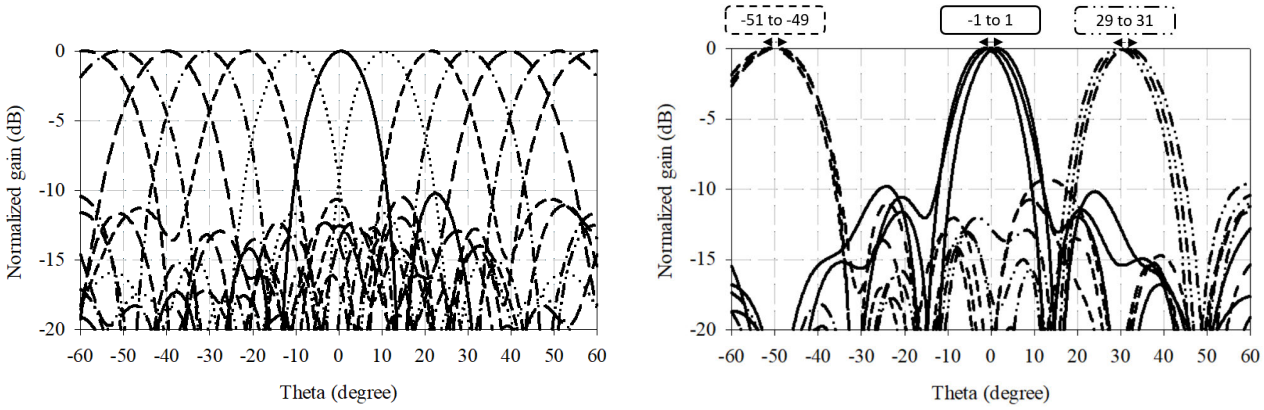

FIGURE 14. Beam steering ability of the proposed 8-element phased array system: (a) calculated beam steering of the 8-element antenna pattern with 10° step and (b) fine beam steering with 1° step based on the measured S-parameters data.

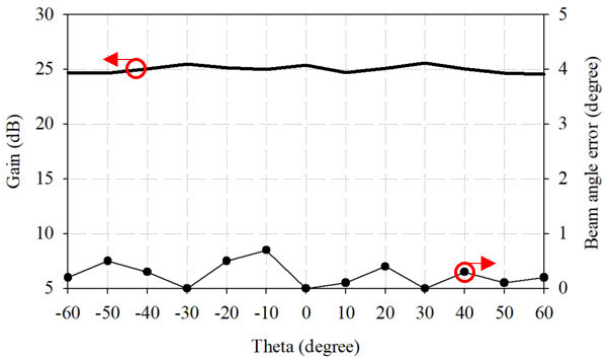

FIGURE 15. Calculated results of gain and beam angle error of proposed 8-element phased array system based on the measured S-parameters.

equal to $G_{VSPS,M}$. As shown in (38), the power decreases by 1/4 (-6 dB), resulting in a total output power reduction of 1/8 (-9 dB). For the system using conventional phase shifters, $G_{CH,M} = G_{VGA,M}$. As indicated in (40), the power does not decrease; thus, the total output power is 1/2 (-3 dB) lower.

To summarize, Table 1 shows the system loss comparison of three different phased array systems with two scenarios, beam steering (Case1 and Case2) and beam-width control (Case3 and Case4). The table reveals that the proposed method can achieve the least system loss among the three systems in each case, indicating its ability to deliver a higher system gain. The proposed phased array system also offers the advantage of an improved power budget because it can generate unequal output signals without wasting power.

V. EXPERIMENTAL RESULTS

To demonstrate the proposed phased array system, this study implemented a 3.5 GHz phased array system. The components were fabricated on FR-4 printed circuit boards ($\varepsilon_r = 4.2$, $\tan\delta = 0.02$, and thickness = 0.8 mm).

A. 8 × 8 PHASE MATRIX NETWORK

Figs. 10 depicts the circuit photograph and measured electrical responses of the proposed 8 × 8 phase matrix network. The network was constructed using couplers, crossover circuits, and delay lines. The couplers and crossover circuits are essential components for wideband performance. Thus, second-order branch line couplers were chosen and the crossover circuits were implemented using the mode conversion technique between microstrip lines and coplanar waveguide lines. The delay lines in the 8 × 8 phase matrix network were applied to indicate the equal phase delay to each cascade coupler.

The measured transmission coefficients of S-parameters between the input ports (port 1 to port 8) and output ports (port 9 to port 16) are presented in Figs. 10(b) and (c). In the frequency range of 3.1–3.9 GHz, the average loss with added back the 9 dB theoretical distribution loss is 4 dB, and the amplitude imbalance between each transmission coefficient is ±1.7 dB. The maximum phase error of the normalized phase delay from the input port (Port 1 to Port 8) to the output port (Port 9 to Port 16) is ±10.6°.

B. 1-TO-2 TUNABLE AMPLIFIER AND INVERTER

The circuit photo of the 1-to-2 tunable amplifier is depicted in Fig. 11(a). The $BJT_{A\&B}$ used in the 1-to-2 tunable amplifier was the commercial component (BFU630F, NXP Semiconductors). Data regarding the measured normalized power sum $((|S_{21}|^2+|S_{31}|^2)/G^2_{max})$ under different R settings (power difference of 0.5 dB per step) are presented in Fig. 11(b). The control voltage (Vbb_A and Vbb_B) ranged from 2 V to 0 V per 0.03 V step, which is similar to the same amount of adjustment as a 6-bit control. At 3.5 GHz, the maximum power difference error is 0.2 dB, and the maximum power sum imbalance is 0.3 dB with less than 30 mW power consumption. It is worth mentioning that the 1-to-2 tunable amplifier can be continually fine-tuned and the error of power sum and differences can be minimized.

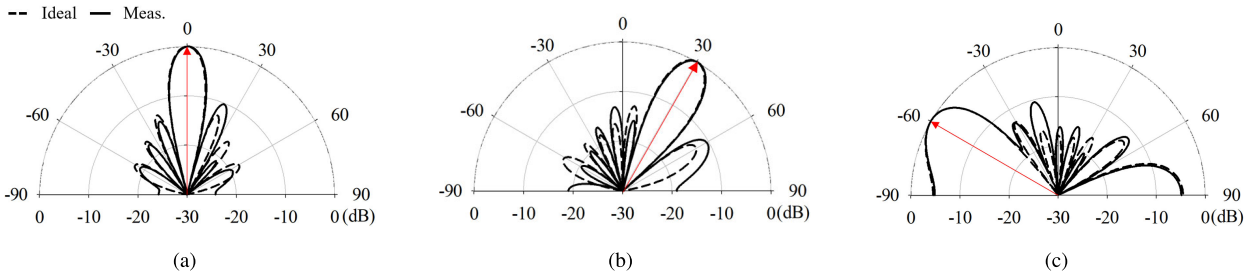

FIGURE 16. Normalized sum beam patterns compare with the ideal sum beam pattern. The direction is aimed at (a) 0°, (b)30°, and (c)−60°.

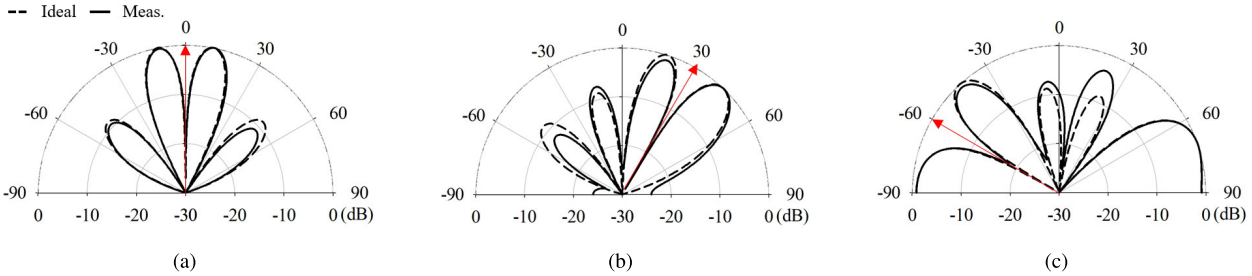

FIGURE 17. Normalized difference beam patterns compare with the ideal difference beam pattern. The direction is aimed at (a) 0°, (b)30°, and (c)−60°.

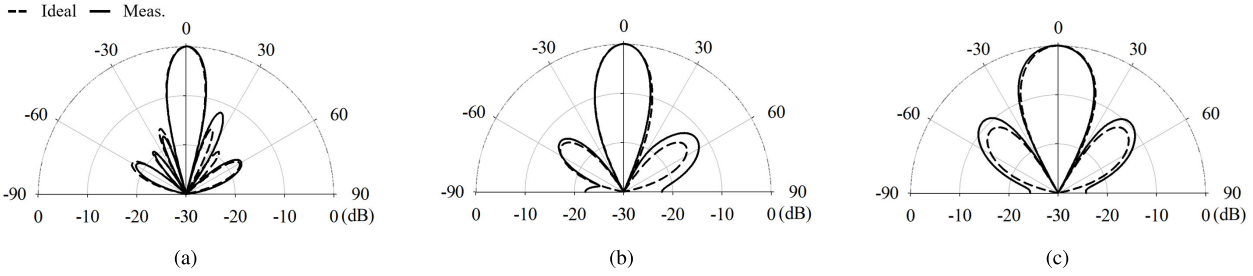

FIGURE 18. Normalized beam tapering patterns compare with the ideal beam patterns at 0°. The power ratio to eight antenna is (a) 0.8/ 0.8/ 1.0/ 1.0/ 1.0/ 1.0/ 0.8/ 0.8 (b)0.2/ 0.2/ 1.0/ 1.0/ 1.0/ 1.0/ 0.2/ 0.2 (c)0.0/ 0.0/ 1.0/ 1.0/ 1.0/ 1.0/ 0.0/ 0.0.

The circuit photo of the inverter is displayed in Fig. 12(a); the inverter comprised a commercial balun (4400BL15A0100E, Johanson Technology) and switch (F2976NEGK8, Integrated Device Technology, Inc.). The results regarding the measured magnitude and phase for States 1 and 2 are illustrated in Fig. 12(b). Over the frequency range of 3.1-3.9 GHz, the maximum magnitude difference is 0.8 dB and a maximum phase deviation is 11.2° (from 180°) can be observed.

C. SYSTEM PERFORMANCES

The beam patterns generated by the proposed system were calculated with the array factors ($\sum_{n=9}^{16} \frac{b_n}{S_{IN}} e^{j2\pi d \sin\theta_d/\lambda}$) which were determined from the measured S-parameters and the half-wavelength antenna spacing. It was equivalent to the phased array with a 0 dBi antenna element. The system gains were based on the transmission coefficients of S-parameters (b_n/S_{IN}) and the peak value of the array factors.

As displayed in Fig. 13, the proposed 8 × 8 phase matrix network and weighting network 1-to-2 tunable amplifiers and phase inverters) were configured to realize the proposed 8-element phased array system and to validate the proposed matrix-sum method for beam steering and beam-width control.

Figs. 14 and 15 present the beam steering capabilities and performances of the proposed 8-element antenna array. As illustrated in Fig. 14(a), the beam steering performance of the system was evaluated in a range of −60° to 60° in steps of 10°. In Fig. 14(b), the beam steering accuracy of the proposed system has been demonstrated by selecting and displaying beam angles from −51° to −49°, −1° to 1°, and 29° to 31° in beam angle steps of 1°. The beam angle deviation and system gains are shown in Fig. 15. The beam angle error is less than 0.7°, and the average system gain is 25.1 dB. These results indicate that when errors from the phase matrix network lead to (2) not being satisfied, the proposed method has the ability to utilize the weighting network to adjust the corresponding

TABLE 2. Comparison table of the 8-element phased array topology that uses three different methods with the same control bit.

Method	Ideal system gain (dB)	Beam angle error in 1° beam accuracy	Ideal system loss of beam steering (sum and difference patterns) (dB)	Ideal system loss of beam-width control with the output amplitude ratio 0:0:0:1:1:0:0:0 (dB)
Conventional phase shifters	$(G_1 - 2L)^a$	0.8°	0	6
Vector-sum phase shifters	$(G_2 - 2L - 6)^b$	0.6°	6	12
Matrix-sum method	$\mathbf{(3G_3 - 2L)^c}$	$\mathbf{0.2^\circ}$	**0**	**0**

[a]: G_1 is the magnitude controller, 2L is the input power divider and conventional phase shifter.
[b]: G_2 is the magnitude controller, 2L is the input power divider and phase inverter, and -6 is the ideal loss of the vector-sum phase shifter.
[c]: G_3 is the 1-to-2 tunable amplifier, 2L is the phase inverter and phase matrix network.

weights and synthesize the acceptable output beams if the errors do not dominate the performance of the phase matrix.

To clearly illustrate the difference between calculated and ideal beams in different cases, three cases with different beam patterns are chosen. The dashed lines in the figures indicate the ideal beam patterns including sum, difference, and tapering patterns, which were generated by an 8-element phased array antenna with no amplitude or phase error. The red arrow indicates the setting of the desired beam angle.

As shown in Figs. 16, the discrepancy in the beam angle is less than 0.5°, and for the first side lobe level error is less than 3 dB. For the difference pattern in Figs. 17, the discrepancy of the null angle is less than 0.3°, and the peak-to-null ratio is larger than 18 dB. The results of beam-width control with non-linear output weighting are shown in Figs. 18. The discrepancy of the beam angle is less than 0.8°, and the half-power beam-width error is less than 1.6°.

Table 2 presents a comparative analysis of the system performance among three 8-element phased array systems employing different beam control methods. Since this work focuses on proving the proposed concept, only the performance dominated with the system topologies was considered. The comparison revealed that the proposed method had the highest beam angle accuracy and lowest system loss in each case and the gain of the proposed system outperforms the two alternative methods when employing the same gain components ($G_1 = G_2 = G_3$).

VI. CONCLUSION

An 8-element phased array system with a novel beam control method, namely, matrix-sum method, capable of beam steering and beam-width control, has been presented and successfully demonstrated. The proposed phased array system comprises a novel 8×8 phase matrix network and a weighting network. Based on validations, it has been established that when utilized with an appropriate phase matrix network, the weighting network requires only real number weightings that can achieve different beam cases. Compared with traditional phased array systems that use conventional phase shifters and amplitude controllers or vector-sum phase shifters, the proposed system was noted to achieve the highest beam angle accuracy (beam angle error less than 0.2°) for the same number of control bits for the weighting network; it could also achieve the lowest system loss (ideally, 0 dB loss) for various beam cases. Moreover, the proposed architecture utilizes a series gain approach, resulting in the highest gain output with the same gain components. The proposed phased array successfully demonstrates $\pm 60^\circ$ beam steering range and beam accuracy in 1° beam steps. The system gain flatness is less than ± 0.5 dB within the entire steering range and the average system gain of the fabricated system, calculated by measured S-parameters data, is 25.1 dB at 3.5 GHz. Compare with ideal beam pattern with different beam cases. The side lobe level is higher than 10 dB for the sum pattern and the peak-to-null ratio is larger than 18 dB for the difference pattern. The results for the beam-width control function are also similar to the ideal beam pattern. The proposed system has undergone comprehensive mathematical verification and has shown promising results in implementation on an eight-element antenna array system.

APPENDIX

A. DIFFERENCE BEAM PATTERN

The weighting value for an excited difference pattern can be determined as follows: The output signals (b_9–b_{16}) are defined as in (21), and ϕ is calculated from the null-point angle θ_n

$$\phi = \frac{2\pi d \sin\theta_n}{\lambda}, \tag{43}$$

subsequently, using (2), (9), (21), and (43), we can derive the input signal a_1–a_8 as

$$\begin{aligned}
a_1 &= |a_1|e^{-j\theta_1} = \frac{k \cdot e^{j\alpha}}{8L_{PMN}}(A_1 + jB_1) \\
A_1 &= 1 + \sin\phi + \sin 2\phi - \cos 3\phi \\
&\quad - \sin 4\phi + \cos 5\phi + \cos 6\phi + \sin 7\phi \\
B_1 &= \cos\phi + \cos 2\phi + \sin 3\phi \\
&\quad - \cos 4\phi - \sin 5\phi - \sin 6\phi + \cos 7\phi
\end{aligned} \tag{44}$$

$$\begin{aligned}
a_2 &= |a_2|e^{-j\theta_2} = \frac{k \cdot e^{j\alpha}}{8L_{PMN}}(A_2 + jB_2) \\
A_2 &= -\cos\phi - \cos 2\phi - \sin 3\phi \\
&\quad - \cos 4\phi - \sin 5\phi - \sin 6\phi + \cos 7\phi \\
B_2 &= 1 + \sin\phi + \sin 2\phi - \cos 3\phi \\
&\quad + \sin 4\phi - \cos 5\phi - \cos 6\phi - \sin 7\phi
\end{aligned} \tag{45}$$

$$
\begin{aligned}
\mathrm{a}_3 &= |a_3|e^{-j\theta_3} = \frac{k\cdot e^{j\alpha}}{8L_{PMN}}(A_3 + jB_3)\\
A_3 &= -\cos\phi + \cos 2\phi + \sin 3\phi\\
&\quad + \cos 4\phi + \sin 5\phi - \sin 6\phi + \cos 7\phi\\
B_3 &= 1 + \sin\phi - \sin 2\phi + \cos 3\phi\\
&\quad - \sin 4\phi + \cos 5\phi - \cos 6\phi - \sin 7\phi
\end{aligned} \tag{46}
$$

$$
\begin{aligned}
\mathrm{a}_4 &= |a_4|e^{-j\theta_4} = \frac{k\cdot e^{j\alpha}}{8L_{PMN}}(A_4 + jB_4)\\
A_4 &= -1 - \sin\phi + \sin 2\phi - \cos 3\phi\\
&\quad - \sin 4\phi + \cos 5\phi - \cos 6\phi - \sin 7\phi\\
B_4 &= -\cos\phi + \cos 2\phi + \sin 3\phi\\
&\quad - \cos 4\phi - \sin 5\phi + \sin 6\phi - \cos 7\phi
\end{aligned} \tag{47}
$$

$$
\begin{aligned}
\mathrm{a}_5 &= |a_5|e^{-j\theta_5} = \frac{k\cdot e^{j\alpha}}{8L_{PMN}}(A_5 + jB_5)\\
A_5 &= \cos\phi - \cos 2\phi + \sin 3\phi\\
&\quad + \cos 4\phi - \sin 5\phi + \sin 6\phi + \cos 7\phi\\
B_5 &= 1 - \sin\phi + \sin 2\phi + \cos 3\phi\\
&\quad - \sin 4\phi - \cos 5\phi + \cos 6\phi - \sin 7\phi
\end{aligned} \tag{48}
$$

$$
\begin{aligned}
\mathrm{a}_6 &= |a_6|e^{-j\theta_6} = \frac{k\cdot e^{j\alpha}}{8L_{PMN}}(A_6 + jB_6)\\
A_6 &= -1 + \sin\phi - \sin 2\phi - \cos 3\phi\\
&\quad - \sin 4\phi - \cos 5\phi + \cos 6\phi - \sin 7\phi\\
B_6 &= \cos\phi - \cos 2\phi + \sin 3\phi\\
&\quad - \cos 4\phi + \sin 5\phi - \sin 6\phi - \cos 7\phi
\end{aligned} \tag{49}
$$

$$
\begin{aligned}
\mathrm{a}_7 &= |a_7|e^{-j\theta_7} = \frac{k\cdot e^{j\alpha}}{8L_{PMN}}(A_7 + jB_7)\\
A_7 &= -1 + \sin\phi + \sin 2\phi + \cos 3\phi\\
&\quad + \sin 4\phi + \cos 5\phi + \cos 6\phi - \sin 7\phi\\
B_7 &= \cos\phi + \cos 2\phi - \sin 3\phi\\
&\quad + \cos 4\phi - \sin 5\phi - \sin 6\phi - \cos 7\phi
\end{aligned} \tag{50}
$$

$$
\begin{aligned}
\mathrm{a}_8 &= |a_8|e^{-j\theta_8} = \frac{k\cdot e^{j\alpha}}{8L_{PMN}}(A_8 + jB_8)\\
A_8 &= -\cos\phi - \cos 2\phi + \sin 3\phi\\
&\quad + \cos 4\phi - \sin 5\phi - \sin 6\phi - \cos 7\phi\\
B_8 &= -1 + \sin\phi + \sin 2\phi + \cos 3\phi\\
&\quad - \sin 4\phi - \cos 5\phi - \cos 6\phi + \sin 7\phi
\end{aligned} \tag{51}
$$

After substituting the new a_1–a_8 and b_9–b_{16} into (20), $|(A_m, B_m) - (A_n, B_n)|$ is zero. This result shows that the phase difference between a_1–a_8 can only be either 0° or 180°.

B. BEAM-WIDTH CONTROL

For an excited beam-width control pattern with nonlinear weighting, (2), (9), (11), and (22) can be used to derive the input signal a_1–a_8 as

$$
\begin{aligned}
\mathrm{a}_1 &= |a_1|e^{-j\theta_1} = \frac{k\cdot e^{j\alpha}}{8L_{PMN}}(A_1 + jB_1)\\
A_1 &= m_1 + m_2\sin\phi + m_3\sin 2\phi - m_4\cos 3\phi\\
&\quad + m_4\sin 4\phi - m_3\cos 5\phi - m_2\cos 6\phi\\
&\quad - m_1\sin 7\phi\\
B_1 &= m_2\cos\phi + m_3\cos 2\phi + m_4\sin 3\phi\\
&\quad + m_4\cos 4\phi + m_3\sin 5\phi + m_2\sin 6\phi\\
&\quad - m_1\cos 7\phi
\end{aligned} \tag{52}
$$

$$
\begin{aligned}
\mathrm{a}_2 &= |a_2|e^{-j\theta_2} = \frac{k\cdot e^{j\alpha}}{8L_{PMN}}(A_2 + jB_2)\\
A_2 &= -m_2\cos\phi - m_3\cos 2\phi - m_4\sin 3\phi\\
&\quad + m_4\cos 4\phi + m_3\sin 5\phi + m_2\sin 6\phi\\
&\quad - m_1\cos 7\phi\\
B_2 &= m_1 + m_2\sin\phi + m_3\sin 2\phi - m_4\cos 3\phi\\
&\quad - m_4\sin 4\phi + m_3\cos 5\phi + m_2\cos 6\phi\\
&\quad + m_1\sin 7\phi
\end{aligned} \tag{53}
$$

$$
\begin{aligned}
\mathrm{a}_3 &= |a_3|e^{-j\theta_3} = \frac{k\cdot e^{j\alpha}}{8L_{PMN}}(A_3 + jB_3)\\
A_3 &= -m_2\cos\phi + m_3\cos 2\phi + m_4\sin 3\phi\\
&\quad - m_4\cos 4\phi - m_3\sin 5\phi + m_2\sin 6\phi\\
&\quad - m_1\cos 7\phi\\
B_3 &= m_1 + m_2\sin\phi - m_3\sin 2\phi + m_4\cos 3\phi\\
&\quad + m_4\sin 4\phi - m_3\cos 5\phi + m_2\cos 6\phi\\
&\quad + m_1\sin 7\phi
\end{aligned} \tag{54}
$$

$$
\begin{aligned}
\mathrm{a}_4 &= |a_4|e^{-j\theta_4} = \frac{k\cdot e^{j\alpha}}{8L_{PMN}}(A_4 + jB_4)\\
A_4 &= -m_1 - m_2\sin\phi + m_3\sin 2\phi - m_4\cos 3\phi\\
&\quad + m_4\sin 4\phi - m_3\cos 5\phi + m_2\cos 6\phi\\
&\quad + m_1\sin 7\phi\\
B_4 &= -m_2\cos\phi + m_3\cos 2\phi + m_4\sin 3\phi\\
&\quad + m_4\cos 4\phi + m_3\sin 5\phi - m_2\sin 6\phi\\
&\quad + m_1\cos 7\phi
\end{aligned} \tag{55}
$$

$$
\begin{aligned}
\mathrm{a}_5 &= |a_5|e^{-j\theta_5} = \frac{k\cdot e^{j\alpha}}{8L_{PMN}}(A_5 + jB_5)\\
A_5 &= m_2\cos\phi - m_3\cos 2\phi + m_4\sin 3\phi\\
&\quad - m_4\cos 4\phi + m_3\sin 5\phi - m_2\sin 6\phi\\
&\quad - m_1\cos 7\phi\\
B_5 &= m_1 - m_2\sin\phi + m_3\sin 2\phi + m_4\cos 3\phi\\
&\quad + m_4\sin 4\phi + m_3\cos 5\phi - m_2\cos 6\phi\\
&\quad + m_1\sin 7\phi
\end{aligned} \tag{56}
$$

$$
\begin{aligned}
\mathrm{a}_6 &= |a_6|e^{-j\theta_6} = \frac{k\cdot e^{j\alpha}}{8L_{PMN}}(A_6 + jB_6)\\
A_6 &= -m_1 + m_2\sin\phi - m_3\sin 2\phi - m_4\cos 3\phi\\
&\quad + m_4\sin 4\phi + m_3\cos 5\phi - m_2\cos 6\phi\\
&\quad + m_1\sin 7\phi\\
B_6 &= m_2\cos\phi - m_3\cos 2\phi + m_4\sin 3\phi\\
&\quad + m_4\cos 4\phi - m_3\sin 5\phi + m_2\sin 6\phi\\
&\quad + m_1\cos 7\phi
\end{aligned} \tag{57}
$$

$$
\begin{aligned}
\mathrm{a}_7 &= |a_7|e^{-j\theta_7} = \frac{k\cdot e^{j\alpha}}{8L_{PMN}}(A_7 + jB_7)\\
A_7 &= -m_1 + m_2\sin\phi + m_3\sin 2\phi + m_4\cos 3\phi\\
&\quad - m_4\sin 4\phi - m_3\cos 5\phi - m_2\cos 6\phi\\
&\quad + m_1\sin 7\phi\\
B_7 &= m_2\cos\phi + m_3\cos 2\phi - m_4\sin 3\phi\\
&\quad - m_4\cos 4\phi + m_3\sin 5\phi + m_2\sin 6\phi\\
&\quad + m_1\cos 7\phi \qquad (58)\\
\mathrm{a}_8 &= |a_8|e^{-j\theta_8} = \frac{k\cdot e^{j\alpha}}{8L_{PMN}}(A_8 + jB_8)\\
A_8 &= -m_2\cos\phi - m_3 cos2\phi + m_4\sin 3\phi\\
&\quad - m_4\cos 4\phi + m_3\sin 5\phi + m_2\sin 6\phi\\
&\quad + m_1\cos 7\phi\\
B_8 &= -m_1 + m_2\sin\phi + m_3\sin 2\phi + m_4\cos 3\phi\\
&\quad + m_4\sin 4\phi + m_3\cos 5\phi + m_2\cos 6\phi\\
&\quad - m_1\sin 7\phi \qquad (59)
\end{aligned}
$$

After substituting the new a_1–a_8 and b_9–b_{16} into (20), $|(A_m, B_m) - (A_n, B_n)|$ is zero. This result shows that the phase difference between a_1–a_8 only be 0° or 180°.

REFERENCES

[1] 4gamericas. (Oct. 2012). *MIMO and Smart Antennas for MobileBroadband Systems*. [Online]. Available: http://www.4gamericas.com

[2] J.-H. Kim, J.-H. Han, J.-S. Park, and J.-G. Kim, "Design of phased array antenna for 5G mm-wave beamforming system," in *Proc. IEEE 5th Asia–Pacific Conf. Antennas Propag. (APCAP)*, Jul. 2016, pp. 201–202.

[3] A. K. Pandey, "Design of a compact high power phased array for 5G FD-MIMO system at 29 GHz," in *Proc. Asia–Pacific Microw. Conf. (APMC)*, Dec. 2016, pp. 1–4.

[4] I. Uchendu and J. R. Kelly, "Survey of beam steering techniques available for millimeter wave applications," *Prog. Electromagn. Res. B*, vol. 68, pp. 35–54, 2016.

[5] S. Kwak, J. Chun, D. Park, Y. K. Ko, and B. L. Cho, "Asymmetric sum and difference beam pattern synthesis with a common weight vector," *IEEE Antennas Wireless Propag. Lett.*, vol. 15, pp. 1622–1625, 2016.

[6] J. E. Stailey and K. D. Hondl, "Multifunction phased array radar for aircraft and weather surveillance," *Proc. IEEE*, vol. 104, no. 3, pp. 649–659, Mar. 2016.

[7] D. Jackson, "Phased array antenna handbook (third edition) [book review]," *IEEE Antennas Propag. Mag.*, vol. 60, no. 6, pp. 124–128, Dec. 2018.

[8] S.-M. Moon, S. Yun, I.-B. Yom, and H. L. Lee, "Phased array shaped beam satellite antenna with boosted-beam control," *IEEE Trans. Antennas Propag.*, vol. 67, no. 12, pp. 7633–7636, Dec. 2019.

[9] T. Chaloun, L. Boccia, E. Arnieri, M. Fischer, V. Valenta, N. J. G. Fonseca, and C. Waldschmidt, "Electronically steerable antennas for future heterogeneous communication networks: Review and perspectives," *IEEE J. Microw.*, vol. 2, no. 4, pp. 545–581, Oct. 2022.

[10] G. Gultepe, T. Kanar, S. Zihir, and G. M. Rebeiz, "1024-element Ku-band SATCOM phased-array transmitter with 45-dBW single-polarization EIRP," *IEEE Trans. Microw. Theory Techn.*, vol. 69, no. 9, pp. 4157–4168, Sep. 2021.

[11] K. K. W. Low, S. Zihir, T. Kanar, and G. M. Rebeiz, "A 27–31-GHz 1024-element Ka-band SATCOM phased-array transmitter with 49.5-dBW peak EIRP, 1-dB AR, and ±70° beam scanning," *IEEE Trans. Microw. Theory Techn.*, vol. 70, no. 3, pp. 1757–1768, Mar. 2022.

[12] O. Kazan, Z. Hu, L. Li, A. Alhamed, and G. M. Rebeiz, "An 8-channel 5–33-GHz transmit phased array beamforming IC with 10.8–14.7-dBm Psat for C-, X-, Ku-, and Ka-band SATCOM," *IEEE Trans. Microw. Theory Techn.*, vol. 71, no. 5, pp. 2029–2039, May 2023.

[13] R. C. Hansen, *Phased Array Antennas*. Hoboken, NJ, USA: Wiley, 1998.

[14] H. J. Visser, *Array Phased Array Antenna Basics*. Hoboken, NJ, USA: Wiley, 2006.

[15] A. J. Fenn, *Adapt. Antennas Phased Arrays for Radar Communications*. Norwood, MA, USA: Artech House, 2007.

[16] B.-W. Min and G. M. Rebeiz, "Single-ended and differential Ka-band BiCMOS phased array front-ends," *IEEE J. Solid-State Circuits*, vol. 43, no. 10, pp. 2239–2250, Oct. 2008.

[17] E. Cohen, M. Ruberto, M. Cohen, O. Degani, S. Ravid, and D. Ritter, "A CMOS bidirectional 32-element phased-array transceiver at 60 GHz with LTCC antenna," *IEEE Trans. Microw. Theory Techn.*, vol. 61, no. 3, pp. 1359–1375, Mar. 2013.

[18] J. G. Lee, T. H. Jang, G. H. Park, H. S. Lee, C. W. Byeon, and C. S. Park, "A 60-GHz four-element beam-tapering phased-array transmitter with a phase-compensated VGA in 65-nm CMOS," *IEEE Trans. Microw. Theory Techn.*, vol. 67, no. 7, pp. 2998–3009, Jul. 2019.

[19] F. Amin, Y. Liu, Y. Zhao, and S. Hu, "Compact and low-loss phase shifters and multibit phase shifters based on inverted-E topology," *IEEE Trans. Microw. Theory Techn.*, vol. 69, no. 4, pp. 2120–2129, Apr. 2021.

[20] X. Li, H. Fu, K. Ma, and J. Hu, "A 2.4–4-GHz wideband 7-bit phase shifter with low RMS phase/amplitude error in 0.5-μm GaAs technology," *IEEE Trans. Microw. Theory Techn.*, vol. 70, no. 2, pp. 1292–1301, Feb. 2022.

[21] A. Valdes-Garcia, S. T. Nicolson, J.-W. Lai, A. Natarajan, P.-Y. Chen, S. K. Reynolds, J. C. Zhan, D. G. Kam, D. Liu, and B. Floyd, "A fully integrated 16-element phased-array transmitter in SiGe BiCMOS for 60-GHz communications," *IEEE J. Solid-State Circuits*, vol. 45, no. 12, pp. 2757–2773, Dec. 2010.

[22] A. Natarajan, S. K. Reynolds, M.-D. Tsai, S. T. Nicolson, J. C. Zhan, D. G. Kam, D. Liu, Y. O. Huang, A. Valdes-Garcia, and B. A. Floyd, "A fully-integrated 16-element phased-array receiver in SiGe BiCMOS for 60-GHz communications," *IEEE J. Solid-State Circuits*, vol. 46, no. 5, pp. 1059–1075, May 2011.

[23] T.-W. Li and H. Wang, "A millimeter-wave fully integrated passive reflection-type phase shifter with transformer-based multi-resonance loads for 360° phase shifting," *IEEE Trans. Circuits Syst. I, Reg. Papers*, vol. 65, no. 4, pp. 1406–1419, Apr. 2018.

[24] C.-H. Chang, J.-Y. Chen, C.-T. Shen, M.-J. Tsai, and T.-S. Tai, "Reflection-type phase shifter integrated with tunable power attenuation mechanism for sub-6 GHz wireless applications," *IEEE Access*, vol. 10, pp. 115532–115540, 2022.

[25] J. Hu, X. Yang, L. Ge, and H. Wong, "A polarization and beam steering reconfigurable cavity-backed magneto-electric dipole antenna array using reflection-type phase shifter," *IEEE Trans. Antennas Propag.*, vol. 70, no. 1, pp. 296–306, Jan. 2022.

[26] B. Yang, Z. Yu, R. Zhang, J. Zhou, and W. Hong, "Local oscillator phase shifting and harmonic mixing-based high-precision phased array for 5G millimeter-wave communications," *IEEE Trans. Microw. Theory Techn.*, vol. 67, no. 7, pp. 3162–3173, Jul. 2019.

[27] A. Asoodeh and M. Atarodi, "A full 360° vector-sum phase shifter with very low RMS phase error over a wide bandwidth," *IEEE Trans. Microw. Theory Techn.*, vol. 60, no. 6, pp. 1626–1634, Jun. 2012.

[28] Y. Yu, K. Kang, C. Zhao, Q. Zheng, H. Liu, S. He, Y. Ban, L.-L. Sun, and W. Hong, "A 60-GHz 19.8-mW current-reuse active phase shifter with tunable current-splitting technique in 90-nm CMOS," *IEEE Trans. Microw. Theory Techn.*, vol. 64, no. 5, pp. 1572–1584, May 2016.

[29] B. Cetindogan, E. Ozeren, B. Ustundag, M. Kaynak, and Y. Gurbuz, "A 6 bit vector-sum phase shifter with a decoder based control circuit for X-band phased-arrays," *IEEE Microv. Wireless Compon. Lett.*, vol. 26, no. 1, pp. 64–66, Jan. 2016.

[30] J. Zhou, H. J. Qian, and X. Luo, "High-resolution wideband vector-sum digital phase shifter with on-chip phase linearity enhancement technology," *IEEE Trans. Circuits Syst. I, Reg. Papers*, vol. 68, no. 6, pp. 2457–2469, Jun. 2021.

[31] X. Zhu, T. Yang, P.-L. Chi, and R. Xu, "Novel passive vector-sum reconfigurable filtering phase shifter with continuous phase-control and tunable center frequency," *IEEE Trans. Microw. Theory Techn.*, vol. 70, no. 2, pp. 1188–1197, Feb. 2022.

[32] V. Napijalo, "Multilayer 180° hybrid coupler in LTCC technology for 24 GHz applications," in *Proc. Eur. Microw. Conf.*, Oct. 2007, pp. 552–555.

[33] T. Klein, C. Günner, J. Kassner, R. Kulke, and H. Wolf, "Multiple feed per beam networks for Ka-band satellite communication systems in LTCC technology," in *IEEE MTT-S Int. Microw. Symp. Dig.*, Jun. 2011, pp. 1–4.

[34] H. Jia, C. C. Prawoto, B. Chi, Z. Wang, and C. P. Yue, "A 32.9% PAE, 15.3 dBm, 21.6–41.6 GHz power amplifier in 65nm CMOS using coupled resonators," in *Proc. IEEE Asian Solid-State Circuits Conf. (A-SSCC)*, Nov. 2016, pp. 345–348.
[35] T.-H. Fan, Y. Wang, and H. Wang, "A broadband transformer-based power amplifier achieving 24.5-dBm output power over 24–41 GHz in 65-nm CMOS process," *IEEE Microw. Wireless Compon. Lett.*, vol. 31, no. 3, pp. 308–311, Mar. 2021.
[36] D. M. Pozar, *Microwave Engineering*. Hoboken, NJ, USA: Wiley, 1998.

YI-TING LIN (Graduate Student Member, IEEE) was born in Taichung, Taiwan, in 1994. He received the M.S. degree in electrical engineering from the Department of Electrical Engineering, National Chung Cheng University, Chiayi, Taiwan, in 2019. He is currently pursuing the Ph.D. degree with the Institute of Communications Engineering, National Yang Ming Chiao Tung University, Hsinchu, Taiwan. His current research interest includes the design of microwave circuits and systems.

ZUO-MIN TSAI (Senior Member, IEEE) was born in Miaoli, Taiwan, in 1979. He received the B.S. and Ph.D. degrees in communication engineering from the Department of Electrical Engineering, National Taiwan University, Taipei, Taiwan, in 2001 and 2006, respectively. From 2006 to 2011, he was a Postdoctoral Research Fellow with the Graduate Institute of Communication Engineering, National Taiwan University. In 2019, he joined the Institute of Communications Engineering, National Yang Ming Chiao Tung University, Hsinchu, Taiwan, as a Faculty Member, where he is currently an Associate Professor. His current research interest includes the design of microwave integrated circuits and microwave systems.

JEN-MING WU (Senior Member, IEEE) received the B.Sc. degree in electrical engineering from National Taiwan University, Taipei, Taiwan, and the Ph.D. degree in electrical engineering from the University of Southern California. From 1998 to 2003, he was with Sun Microsystems Inc., Sunnyvale, CA, USA, as a member of Technical Staff. Since 2021, he has been jointly appointed as the Director of the Next-Generation Communications Research Center, Hon Hai Research Institute, Taiwan. Since 2003, he has been a Faculty Member with the Department of Electrical Engineering, Institute of Communications Engineering, National Tsing Hua University, Taiwan, where he is currently a Full Professor. He holds more than eight U.S. patents in the field of communications and 14 contributions in 3GPP 5G New Radio and IEEE 802.16m standards meetings. He has published more than 100 technical articles in international journals and conference proceedings. His research interests include communications from theory to practice, including wireless communications signal processing, information and coding theory, MIMO radar signal processing, phased array antenna transceiver IC designs, and wireless system prototypes. He was a recipient of the Best Paper Award from the Taiwan Telecommunications Symposium, in 2008 and 2020, the Outstanding Chapter Award from the IEEE Vehicular Technology Society Taipei Chapter, in 2020, the Achievement Award of the Golden Silicon Award Competition, in 2007 and 2008, and the Bronze Medal of the Taiwan Semiconductor Manufacturing Cooperation (TSMC) Research Program, in 2007. He has served as the Chair of IEEE Vehicular Technology Society Taipei Chapter, from 2020 to 2022, the TPC Chair of IEEE Asia Pacific Wireless Communications Symposium, in 2018, and a TPC Member of IEEE Global Communications Conference (Globecom), IEEE International Communications Conference (ICC), and IEEE Vehicular Technology Conference (VTC). He serves as the Director of the IEEE Taipei Section, from 2021 to 2024.